INVESTIGATIONS OF ATOMIZATION OF DROPLETS IN TURBULENT FLOWS

A Thesis

by

Veli Can Coşar

Submitted to the
Graduate School of Sciences and Engineering
In Partial Fulfillment of the Requirements for
the Degree of

Master of Science

in the
Department of Mechanical Engineering

Özyeğin University
December 2022

INVESTIGATIONS OF ATOMIZATION OF DROPLETS IN TURBULENT FLOWS

Approved by:

Associate Professor Dr-Ing. Özgür Ertunç,
Advisor
Department of Mechanical Engineering
Özyeğin University

Assistant Professor Dr. Altuğ Melik Başol
Department of Mechanical Engineering
Özyeğin University

Professor Dr. Kerem Pekkan
Department of Mechanical Engineering
Koç University

Date Approved: 22 December 2022

To my family and my dear friends

ABSTRACT

Droplets are used in many important technologies, in the form of either single droplets or spray. Examples include car engines, combustion chambers of jet engines, rocket engines, metal particle production, surface coatings, surface cooling, surface reactions, inhalation, inhalation, agricultural spraying and inkjet printing technology. For example, in car, jet and rocket engines, the droplets are exposed to strong turbulent flow and they are divided into smaller pieces (atomization). It is very important to understand the relationship of atomization with the turbulence parameters for the development of relevant technologies and the creation of new technologies.The properties of the liquid, the speed of the droplet and the characteristics of turbulence are effective in the atomization of the liquid drop in the turbulent gas environment. Due to the eddies in the flow, transient forces occur on the droplets. The droplet becomes unstable by the action of these forces and by the interaction of the inner viscous and surface tension forces. Factors related to atomization should be expressed in dimensionless numbers. For example, Weber number of the the droplet, the Reynolds number of the droplet, the Reynolds number of the turbulence, the Ohnesorge number, the ratio of the length scales of the turbulence (Kolmogorov, Taylor and Integral length scales) to the diameter of the drop, the ratio of the average drop size resulting from the atomization to the length scales of the turbulence and the ratio of the time of atomization to the time scales of turbulence are examples of the most important of these dimensionless parameters. In addition, the interaction between turbulence and droplet is only defined with surface tension of the droplet, density and dissipation rate of the flow around it. There should be more parameters as decribed as example

of dimensionless numbers. To have a better understanding of the atomization process, an isotropic homogenous turbulent flow environment is prepared with a cubic shaped wind tunnel. Due to avoid the effect of droplet coalescence and collapsing in breakup process, one droplet is exposed to isotropic turbulence and its breakup is examined. The parameters of turbulent flow are changed within a systematical control by changing speed or velocity profile of the propellers.

ÖZETÇE

Damlalar, gerek tek gerekse sprey şeklinde, birçok önemli teknolojide kullanılmaktadır. Araba motorları, jet motorların yanma odaları, roket motorları, metal parça üretimi, yüzey kaplamaları, yüzey soğutması, yüzey reaksiyonları, solunum yolu ile ilaç alımı, yangın söndürmesi, tarımsal ilaçlama ve inkjet baskı teknolojisi bunlara örnektir. Örneğin araba, jet ve roket motorlarında, damlalar, kuvvetli türbülanslı akışa maruz kalıp daha da küçük parçalara bölünmektedir. Bu parçalanmanın türbülans parametreleri ile olan ilişkisinin anlaşılması, bu konuyla ilgili teknolojilerin geliştirilmesi ve yeni teknolojilerin yaratılması için çok önemlidir. Sıvı damlanın, türbülanslı gaz ortamında parçalanmasında, sıvının özellikleri, damlanın hızı ve türbülansın özellikleri etken olmaktadır. Akıştaki salınımlardan dolayı, damla üstünde kararsız kuvvetler oluşur. Damla bu kuvvetlerin etkisiyle ve damla içi viskoz ve yüzey gerilimi kuvvetlerin etkileşimi ile kararsız şekilde deforme olur ve damla içi kararsız akış oluşur. Parçalanmayla ilgili etkenler, birimsiz sayılarla ifade edilmelidir. Damlanın ataletinin yüzey gerilimi kaynaklı kuvvette oranı olan Weber sayısı, damlanın Reynolds sayısı, türbülansın Reynolds sayısı, Ohnesorge sayısı, türbülansın uzunluk ölçüsünün (Kolmogorov, Taylor ve Integral) damlanın çapına oranı, parçalanma sonucu ortaya çıkan ortalama damla boyutunun türbülansın uzunluk ölçüsüne oranı ve parçalanma zamanın türbülansın zaman ölçüsüne oranı bu sayıların en önemlilerine örnektir. Bunun yanı sıra, damla ve çevresindeki türbülanslı akış arasındaki ilişki sadece damlanın yüzey gerilimi, damlayı taşıyan gazın yoğunluğu ve akışın disipasyon oranı ile açıklanmıştır. Parçalanma sürecini daha iyi anlamak için, izotropik ve homojen özelliklere sahip türbülanslı akışın olduğu küp şekilli bir rüzgar tüneli üretilmiştir. Damlaların kendi

aralarında çarpışmalarını ve bu çarpışmaların parçalanma konusundaki etkisini ortadan kaldırmak için deneyler tek damlanın izotropik türbülans akışına atılıp parçalanmasını gözlemleyerek yapılmıştır. Türbülanslı akışın özellikleri sistematik olarak pervanelerin hızını ve hız profilleri aracılığıyla değiştirilmiştir.

ACKNOWLEDGEMENTS

I appreciate to my advisor, Dr-Ing. Özgür Ertunç for limitless support and help from the beginning to the last moment. I would like to thanks to my family for their endless support and faith and to my friends for their dear friendship.

This study was supported by the Scientific and Technological Research Council of Turkey (TUBITAK), project no:119M087. I would like to thanks them to their economical support.

TABLE OF CONTENTS

DEDICATION . . . . . **iii**

ABSTRACT . . . . . **iv**

ÖZETÇE . . . . . **vi**

ACKNOWLEDGEMENTS . . . . . **viii**

LIST OF TABLES . . . . . **xi**

LIST OF FIGURES . . . . . **xii**

I INTRODUCTION **1**

1.1 Droplet Breakup Phenomenon 2

1.2 Turbulent Effect on the Droplet Breakup 4

1.3 Previous Studies on Isotropic and Homogeneous Turbulence 5

1.4 Open Fields in the Literature 10

1.5 Hypothesis of the Study 11

1.6 Objectives of the Study 11

1.7 Methodology 12

1.8 Structure of the Thesis 13

II NUMERICAL AND ANALYTICAL APPROACH **14**

2.1 Numerical Approach 14

2.2 Analytical Approach 17

2.2.1 Turbulent Kinetic Energy 18

2.2.2 Turbulent Dissipation Rate 20

2.2.3 D_{max} Values 22

2.2.4 Two-point Correlation 23

2.2.5 Isotropy and Homogeneity of the Flow 26

III EXPERIMENTAL FACILITIES **32**

3.1 Design of the Wind Tunnel 32

3.2 Droplet Generation 36
3.3 Calibration Setup for the Hot-wire Experiments 37
IV EXPERIMENTAL RESULTS 39
4.1 Droplet Breakup in the Wind Tunnel 39
4.2 Turbulence Measurements of the Wind Tunnel 50
4.2.1 Calibration of the Hot-wire Probe 51
4.2.2 Hot-wire Measurements in the Wind Tunnel 52
4.2.3 Results of the Hot-wire Measurements 53
V CONCLUSION AND FUTURE RECOMMENDATIONS 58
5.1 General Conclusion 58
5.2 Recommendations for Future Work 60
VITA 65

LIST OF TABLES

1 Breakup types of a droplet in a laminar flow and models of the phenomenon[1] 3

2 The estimation values of Taylor microscale at each experimental condition[2] 6

3 Experimental results of Gökalp and Birouk's setup[3] 7

4 Analytical results of turbulent dissipation rate, D_{max} and Taylor Reynolds number 8

5 Experimental results of Bradley, Lawes and Morsy's setup[4] 8

6 Analytical results of turbulent dissipation rate, D_{max} and Taylor Reynolds number 8

7 Experimental results of Ravi, Peltier and Petersen's setup[5] 9

8 Analytical results of turbulent dissipation rate, D_{max} and Taylor Reynolds number 9

9 Comparison of different approaches about TKE calculation 20

10 Comparison of different approaches about TDR calculation 21

11 Comparison of simulation results with changing in the RPM value and D_{max} results 23

12 Taylor microscale results respect to RPM value of the propellers . . . 26

13 Detailed information about count of the produced droplet and probability of breakup occurrence 41

14 Detailed information about counts of the most probable breakup height and its probability for each scenario 44

15 Probabilities of the droplet breakup types for each scenario 46

LIST OF FIGURES

1 Grid structure of the CFD simulations 15

2 Velocity vector field in 300x300x300 mm cubic test chamber with the propeller speed of a)5000 RPM, b)6000 RPM and c)8000 RPM 16

3 Instantaneous velocity components at center of the 300x300x300 mm cubic test chamber with the propeller speed of a)5000 RPM, b)6000 RPM and c)8000 RPM 17

4 Point probes to collect instantaneous velocity data 18

5 Turbulent kinetic energy in the probes respect to placement of them respect to Eq.10 a)5000 RPM, b)6000 RPM and c)8000 RPM 19

6 PSD curve of the center probe a)5000 RPM, b)6000 RPM and c)8000 RPM 19

7 Turbulent dissipation rate of the three cases; a)5000 RPM, b)6000 RPM and c)8000 RPM 21

8 D_{max} values of the cases; a)5000 RPM, b)6000 RPM and c)8000 RPM 22

9 Two point correlation for isotropic turbulence 24

10 Two-point correlation for 5000 RPM. In left, whole data from all probes is used. In right, the data is averaged respect to its position axis . . . 25

11 Two-point correlation for 5000 RPM with 'f' function. The left graph include all 'r' values.The right graphs use the average value. 25

12 Two-point correlation for 5000 RPM with 'g' function. The left graph include all 'r' values.The right graphs use the average value. 26

13 Anisotropy invariant map from the work of Lumley [6] 27

14 Anisotropy invariant map and results; a) Created AIM for whole regimes, b) AIM for 5000 RPM, c) AIM for 6000 RPM, d) AIM for 8000 RPM 29

15 Isotropy ratio of the 109 data probes; a) 5000 RPM, b) 6000 RPM, c) 8000 RPM 30

16 Homogenity ratio of the 109 data probes; a) 5000 RPM, b) 6000 RPM, c) 8000 RPM 31

17 Corner cubes of the wind tunnel 33

18 Side profiles and assembly manual 33

19 Skeleton of the wind tunnel; a) Front view, b) Isometric view 34

20 Connection between servo motor and propeller; a) Schematic of the assembly of moving parts, b) Parts of the assembly 35

21 Isotropic turbulent flow wind tunnel design in CAD environment; a) Front view, b) Side view 36

22 Isotropic turbulent flow wind tunnel; a) Front view, b) Side view . . . 37

23 Syringe Pump 38

24 Test section for calibration process of the hot-wire system 38

25 Example of two different scenarios a)6000 RPM constant b) sine function varies between 5000-6000 RPM with 1 hertz 39

26 Probability of occurrence of droplet breakup respect to different velocity profiles 40

27 Frame of the collected images with height measuring line 42

28 Probability of the sides where the breakup occurred 43

29 An example of a breakup, directed to the center (speed of the propellers: 3000 RPM, diameter of the droplet: 2.11 mm, type: bag breakup) 43

30 Probability of the height ranges where the breakup occurred in constant speed of propellers 44

31 Probability of the height ranges where the breakup occurred in different velocity profiles 45

32 Probability of the breakup types in constant RPM values 46

33 Probability of the breakup types in different velocity profiles 47

34 An example for a vibrational breakup (speed of the propellers: 5000 RPM, diameter of the droplet: 2.32 mm) 47

35 An example for a hybrid breakup (speed of the propellers: 6000 RPM, diameter of the droplet: 2.19 mm) 48

36 An example for a multi-directed bag breakup (speed of the propellers: 5000-6000 RPM sine func. 2 Hertz, diameter of the droplet: 2.03 mm) 49

37 An example for a multiple breakup (speed of the propellers: 5000-6000 RPM sine func. 1 Hertz, diameter of the droplet: 2.00 mm) 49

38 Placements of hot-wire probe: a) Vertical, b) Horizontal 51

39 Hot-wire calibration curve to be used in converting the voltage to velocity magnitude 52

40 Position of the hot-wire probes: a) Parallel to glass (PG), b) Parallel to cover (PC) 53

41 Voltage data and the obtained velocity magnitudes at the center of the tunnel; a) Voltage data, b) Velocity magnitudes 54

42 Mean velocity and turbulent intensity at the center of the tunnel; a) Mean velocity, b) Turbulent intensity 54

43 Power spectrum density curves of 6000 RPM (PC) case with -5/3 line a) PSD respect to wavenumber, b) PSD respect to frequency 55

44 Turbulent kinetic energy (TKE), uu and turbulent dissipation rate (TDR) values for whole scenarios; a) TKE, b) TDR, c) uu 56

45 Calculated turbulence properties at the center of the tunnel respect to different scenarios; a) Turbulence Reynolds number, b) Taylor Reynolds number, c) Taylor microscale, d) Lengthscale of large eddies 57

Nomenclature

Greek and Roman Symbols

ϵ	Turbulent Dissipation Rate
η	Kolmogorov scale
κ	Wavenumber
λ_f	Longitudinal Taylor Microscale
λ_g	Transverse Taylor Microscale
ν	Kinematic Viscosity
ρ	Density
ρ_a	Density of air
σ	Surface Tension

Other Symbols

δV	Velocity Difference
δ_{ij}	Kronecker Delta
μ	Mean
E	Voltage
$E(\kappa)$	Power Spectrum Density
f	Longitudinal Correlation Function
g	Transverse Correlation Function

H	Homogeneity
k	Turbulent Kinetic Energy
L	Lengthscale($\frac{k^{3/2}}{\epsilon}$)
p	Probability
Re_λ	Taylor Reynolds Number
Re_L	Turbulent Reynolds Number
u'_{rms}	RMS of the Fluctuated Velocity
u_{rms}	RMS of the Velocity
$u_x^{'}$	Fluctuated Velocity at x-axis
$u_y^{'}$	Fluctuated Velocity at y-axis
$u_z^{'}$	Fluctuated Velocity at z-axis
V	Velocity
$We_{turb,crit}$	Critical turbulent Weber Number
z^*	z-score

CHAPTER I

INTRODUCTION

Droplet breakup phenomenon has a vital role in many technological applications such as combustion chambers in cars, jet and liquid fuel rocket engines, powder metal production for additive manufacturing, surface coatings, surface cooling, surface reactions, inhalation drug intake, fire extinguishing, agricultural spraying, and inkjet printing. Because of the wide application area and complexity of the breakup behavior in chaotic environments; many engineers, physicists and mathematicians are working on the behavior of droplet dynamics in turbulent flows.

The most common way to break up a droplet is using an atomizer and creating a spray form throughout environment. For example, in car, jet or rocket engines, combustion chambers have a strong turbulent flow in them which effects the fine droplet particles generated through the use of an injector by further to dividing them into smaller pieces. To enhance and forecast the new products, CFD simulations are utilized with physical model of atomization process which includes properties of liquid, the speed of the droplet and quantities of turbulence. The chaotic nature of turbulence makes it almost impossible to reach an exact solution; therefore, increasing the hardness of estimation of incoming results during breakup process.

In the present work, the experiments concentrate on a single droplet because since the models deal with coalescence, or breakup of droplets by hitting each other. Solving one droplet case successfully may lead to correct the other two breakup effects. In addition, the experimental device is built to create an isotropic and homogenous turbulent flow which can breakup and atomize water or ethanol droplets in diameter of 2 mm, which is considered to be the in the size range of a nearly unstable droplet

diameter and can be easier to break up leading to an easier breakup process. The mean velocity of the flow is nearly zero in a closed environment. The desired turbulent flow is provided from the device with similar principles as known as French Washing Machine in literature [7][8]. Nonetheless, the experimental device uses propellers to push the airflow, not a liquid flow, through each other to build an isotropic, homogenous and zero velocity turbulent environment.

1.1 Droplet Breakup Phenomenon

There are two different atomization class for droplets which are named as primary atomization and secondary atomization [1][9]. Understanding of primary and secondary atomization of a jet flow determines the success of the utilized technology and lead up to new developments. The primary atomization is caused by the force from the used device which is understood quite well and explained with its technological application in the books [9][10][11]. On the other hand, the droplets can breakup into even smaller pieces by the aerodynamic effects of the flow in the environment. The secondary atomization occurs due to the interaction of aerodynamic forces on the droplet and surface tension on the droplet surface, viscous forces and inertia on the droplet which depends on the fluid and flow properties where the drop is located. Most of the studies are done in the laminar flow conditions due to its simplicity when compared with turbulent flow. In a laminar flow, wide range of different breakup types can be observed respect to the generated forces around the droplet. Especially, the Weber number, which is used for investigating the flows where there is an interface between two different fluids, classifies the breakup phenomenon. In addition, Weber number is the ratio of inertia of the droplet and surface tension.

Table 1: Breakup types of a droplet in a laminar flow and models of the phenomenon[1]

Breakup Type	Example of Visual of the Breakup	Weber Number	Model
Vibrational breakup		≈12	TAB, Reitz-Diwakar, SSD
Bag breakup		<20	TAB, Reitz-Diwakar, SSD
Bag/streamer or Bag/Plume breakup		<50	TAB, KHRT, Reitz-Diwakar, SSD
Stripping breakup		<100	KHRT, Reitz-Diwakar, SSD
Catastrophic breakup		>100	KHRT, Reitz-Diwakar, SSD

To investigate the applications in high Mach numbers, equivalent to high Weber numbers, droplets are put into shock tubes to leading to catastrophic breakup [12][13]. These works are mostly for injection in jet engines which flies at speed above hypersonic as ramjet, scramjet and liquid behavior in explosion of chemical bombs. As shown in the figures, the catastrophic breakup type was investigated but a detailed approach cannot be found from only high speed perspective. On the other hand, much detailed work with three different experimental system and many different liquids are done to reach deeper understanding of droplet breakup [14]. Until these experiments, the droplet breakup was explained with Weber number but they found the effect of Ohnesorge number which shows the relation between viscous force, inertia and surface tension of the droplet during breakup process. The Ohnesorge number (Oh) is the ratio of viscous force inside the droplet to the square root of the multiplication of the inertia and surface tension force of the droplet. Higher Ohnesorge number means that the applied force on the droplet is damped with viscosity. For example; water and fuel type liquids have less than 0.1 Oh number that's why the transition in breakup

types occurs in the same We number. However, rising in the Oh number to higher than 0.1 also increases the We number for breakup phenomenon which needs more velocity difference between droplet and the flow around it.

1.2 Turbulent Effect on the Droplet Breakup

The physical interaction between a turbulent flow and a droplet depends on their specific properties respectively. parameters which are the specific properties of them and their movement. The Parameters such as density, viscosity with viscous force, surface tension with surface tension for, size and the relative velocity of the droplet are its own effective quantities. In addition, for a turbulent flow, environment; density, viscosity, mean velocity, intensity, kinetic energy, anisotropy, length scale, time scale and velocity scale affect the whole process during breakup and droplet shapes after breakup. A droplet can be disturbed with its own mean velocity or flow velocity around it even though there is no turbulence. However, the created pressure differencet from the vortices on droplet, viscous shear and normal forces endeavor contribute to breakup while the viscous forces inside the drop and the tension force on its surface prevent the drop from deforming and divided.

The first studies about droplet breakup phenomenon in turbulence focused on emulsion [15] and theoretical approach by Kolmogorov and Hinze [16][17]. Kolmogorov found the biggest particle to be able to break up in a turbulent flow by utilizing dissipation rate theory and modelled it with its constants in liquid-liquid droplet interaction as known as emulsion. From his perspective, Kolmogorov assumed that the droplet can be only divided by vortices which has same or smaller size of vortices. The bigger vortices push the droplet. However, these bigger vortices can provide a velocity magnitude on droplet which can break up the droplet with a mean velocity without turbulent quantities. Also, except for the largest eddy structures in the integral length scale dimensions of turbulence, eddies in the equilibrium

range have as much energy as in Kolmogorov's dissipation model. From his universal equilibrium theory about turbulent flows, the vortices in Kolmogorov scale are isotropic. Turbulent flow with a constant Oh number can breakup a droplet when We number of flow is higher than the critical We number. The critical We number is described as following;

$$We_{turb,crit} = \frac{\rho_a \delta V^2 D_{max}}{\sigma} \tag{1}$$

From Hinze's explanation, D_{max} is the smallest diameter of the breakable droplets. By using Kolmogorov's energy dissipation theory and structural function of vortices, this size relates with average velocity different as below;

$$\delta V^2 = 2(\epsilon D_{max})^{2/3} \tag{2}$$

By putting dissipation rate parameter into the relation of critical turbulent We number;

$$We_{turb,crit} = \frac{\rho_a \epsilon^{2/3} D_{max}^{5/3}}{\sigma} \tag{3}$$

On the other hand, Hinze's and Clay's experiments in emulsion environment describe the relation between surface tension of the droplet, density and dissipation rate of the turbulent flow.

$$D_{max} = 0.725 \left(\frac{\sigma}{\rho_a}\right)^{3/5} \epsilon^{-2/5} \tag{4}$$

The D_{max} value indicates the smallest droplet that can be break up in the turbulent flow.

1.3 Previous Studies on Isotropic and Homogeneous Turbulence

There are several experiments about creating isotropic and homogeneous flow and one of the methods is French Washing Machine in the literature. These studies generally

focus on combustion chambers, flame speeds or experiments on measuring turbulent quantities but the recent work leads to a new approach. The speed, blade count, shape and number of the propellers affect all turbulent conditions. In order to optimize the literature reviewing process, the research area is narrowed down to reach and compare the most relevant information.

The length scales in turbulence is an important aspect of the design conditions according to works of Kolmogorov which claims that the droplet can be only influenced by vortices smaller or same sized as the droplet. Therefore, the works which observes nearly or smaller than 2 mm in Taylor microscale, are investigated with the changing on RPM values. Previous experiments did not find an exact relation between speed of propeller and eddy sizes in the flow. However, the propellers with higher speeds generate a turbulent flow with lower eddy sizes according to work of Xu [2].

Table 2: The estimation values of Taylor microscale at each experimental condition[2]

Rotational Speed (RPM)	Pressure (MPa)					
	0.1	0.75	1.0	1.5	2.3	3.0
1000	-	-	-	0.410	0.332	0.292
1500	-	0.469	0.406	0.332	0.269	0.236
2000	-	0.405	0.351	0.287	0.232	0.204
2500	-	0.361	0.313	0.256	0.207	0.182
2900	0.915	0.335	0.290	0.237	0.192	0.169

On the other hand, size of the test chamber changes the turbulent parameters as well as speed of propellers. The combination of these two effects can lead the design to a certain designing stage. Therefore, the most probable setups due to its sizes and simplicity, are selected in three works and investigated analytically to find the D_{max} value with Hinze's explanation for water and ethanol. The analytical calculations are made according to Pope's book which describes Turbulent Reynolds Number, Taylor Reynolds number, and the ratios between different length scales[18]. The turbulent

Reynolds number;

$$Re_L \equiv \frac{k^{1/2}L}{\nu} = \frac{k^2}{\epsilon\nu} \tag{5}$$

Taylor Reynolds Number;

$$Re_\lambda = (\frac{20}{3}Re_L)^{1/2} \tag{6}$$

Taylor microscale and Kolmogorov Scale

$$\eta/L = Re_L^{-3/4} \tag{7}$$

$$\lambda_g/L = \sqrt{10}{Re_L}^{-3/4} \tag{8}$$

$$\lambda_g = \lambda_f/\sqrt{2} \tag{9}$$

In the study by Gökalp and Birouk, a cubic shaped box, 400x400x400 mm, was built with eight five-bladed fans and operated between 750 and RPM [3]. Although the main purpose of the experimental setup is to investigate the turbulence effect in the evaporation of different types of liquid drops, the turbulence parameters calculated as a result of the measurements made in the setup.

Table 3: Experimental results of Gökalp and Birouk's setup[3]

N (rpm)	k (m^2/s^2)	L (mm)	λ (mm)	η (mm)	Re_L
750	0.10	8.10	4.90	0.20	31
1070	0.21	8.60	4.20	0.16	45
1450	0.36	8.30	3.60	0.13	59
1800	0.58	8.90	3.30	0.11	75
2270	0.85	8.60	2.90	0.10	90
2700	1.45	8.90	2.60	0.08	118

Table 4: Analytical results of turbulent dissipation rate, D_{max} and Taylor Reynolds number

N (rpm)	ε (m^2/s^3)	D_{max} water (cm)	D_{max} ethanol (cm)	Re_λ
750	21.42	3.99	1.95	14.38
1070	65.07	2.56	1.25	17.32
1450	145.86	1.85	0.90	19.83
1800	297.83	1.39	0.68	22.36
2270	533.05	1.10	0.54	24.49
2700	1183.12	0.80	0.39	28.05

In the experiment by Bradley, Lawes and Morsy, a sphere geometry with an inner diameter of 380 mm and four eight-blade fans of 75 mm length and 72 mm diameter were operated in the range of 1000-6000 rpm[4]. In this experiment, the properties of the turbulent flow environment were examined, and important information was obtained. The vortex scale in the table was found by calculating the scalar size of the directional vortex scale.

Table 5: Experimental results of Bradley, Lawes and Morsy's setup[4]

N (rpm)	Re_L	Re_λ	L (mm)	λ (mm)	$\eta \times 5$ (mm)
1000	1615	220.2	30.4	2.01	0.88
2000	3360	317.4	32.58	1.08	0.51
3000	4943	385.0	32.36	0.73	0.38
4000	6300	434.9	31.69	0.53	0.30
5000	7956	488.7	31.38	0.44	0.26
6000	10274	555.4	33.06	0.38	0.23

Table 6: Analytical results of turbulent dissipation rate, D_{max} and Taylor Reynolds number

N (rpm)	ε (m^2/s^3)	D_{max} water (cm)	D_{max} ethanol (cm)
1000	21.42	4.40	2.14
2000	65.07	2.04	0.99
3000	145.86	1.27	0.62
4000	297.83	0.92	0.45
5000	533.05	0.68	0.33
6000	1183.12	0.55	0.27

Experiments were conducted by Ravi, Peltier and Petersen to examine the differences created by the number and angle of blades on the propeller[5]. In these experiments, a cylinder with an inner diameter of 30.5 cm and a length of 35.6 cm was used. Four fans were chosen to stand opposite each other on the four sides of the cylinder. The distance between the fans standing opposite each other is 20.32 cm. All scenarios took place at the same propeller speed (8300 RPM). Selected fans have three or six blades, 20° or 60° blade angle. In the comparison process, the model with three blades and a blade angle of 20° was used and compared with other scenarios. The purpose of this experiment process is to examine and compare the turbulence characteristics within the apparatus, as in the previous experiment

Table 7: Experimental results of Ravi, Peltier and Petersen's setup[5]

No. of Blades - Angle	ε (m^2/s^3)	Re_λ	L (mm)	λ (mm)	η (mm)
3 blades – 20°	59.7	277	54	2.9	0.1
6 blades – 20°	57.5	218	38	2.6	0.1
3 blades – 60°	109.7	245	39	0.4	0.1

Table 8: Analytical results of turbulent dissipation rate, D_{max} and Taylor Reynolds number

No. of Blades - Angle	D_{max} water (cm)	D_{max} ethanol (cm)
3 blades – 20°	2.65	1.29
6 blades – 20°	2.69	1.31
3 blades – 60°	2.65	1.29

As a result of the extensive literature search, it was understood that none of the studies selected with the highest dissipation rates could breakup a droplet with a diameter of 2 mm. The closest possible result is that the system used in the experiment done by Bradley, Lawes and Morsy has the flow condition to break up an ethanol drop with a diameter of 2.7 mm in the scenario operated at 6000 RPM. The inadequacies of the systems can be explained by the size of the flow volume they

use and the smallness of their propellers. The planned system will have a smaller flow medium and larger propellers than these experiments. Extending the length of the propeller will increase the air drawn from the rear and have a flow environment that accelerates as it approaches the propeller. In addition, the cases created in the experiments may cause the propellers to rotate only in one direction and only push the flow towards the center.

1.4 Open Fields in the Literature

The work of Hinze must be corrected by changing the turbulent quantities systematically by measuring the turbulence. On the other, creating different turbulent conditions can test the Hinze's theory and show the difference with real life. By observing the error and being sure about several experiments, a new effect can be added into a model according to the results of droplet breakup.

In the literature, there are a few DNS works on single droplet investigation of Shao which observes stochastic vibrational effects on breakup process and multiple droplets from Dodd's work even the model has coalescence and collapsing effects of droplets[19][20].

The studies of between gas and liquid droplet interaction are only made with a flow with certain direction which means that there is a velocity magnitude on an axis[21][22].However, without a mean flow, whole generated energy is caused by fluctuations of velocity which feeds the turbulence. On the other hand, the flow structures occurred because of velocity gradients and observing turbulence effects become more clearly.

To create an isotropic and homogenous turbulence, many works are similar to each other according to usage of flow sources in opposite direction. The selected examples with enough data to calculate the turbulent dissipation rate for finding D_{max} of the droplet, has not sufficient turbulent energy to breakup a 2 mm droplet[3][4][5].

Because their experiments do not aim to achieve any breakup capability. Despite that, there are many useful knowledge about effect of size of the closed shape, propeller shape and blade number, RPM value and distance between propellers.

1.5 Hypothesis of the Study

The size of the largest unbreakable droplets cannot depend solely on the dissipation rate according to Eq-4. There should be more parameters to be added into model. The ratio of the vortex size distribution to the droplet diameter, the ratio of the time scale of turbulence to time scale of surface tension of the droplet, the energy distribution of vortices and the time of the droplet spends in the turbulence effect the breakup behavior of the droplet. To summarize, the breakup time and sizes of droplets after breakup should be a function of Taylor Reynolds Number and the ratio of diameter of the droplet to Taylor length scale.

1.6 Objectives of the Study

The objectives of the study are as follows:

- The main objective is to generate new approaches of droplet breakup in the turbulent flow conditions by finding different effective parameters during process.
- Consturcting an experimental setup to create isotropic, homogenous and zero mean velocity turbulence.
- Measuring the velocity data in the system to define turbulent quantities.
- Observing and analyzing the droplet atomization in different and well defined turbulent environment.
- Collecting data about size of the droplet after breakup, the droplet distribution, the breakup time of the droplet and type of the breakup.

1.7 Methodology

To determine the parts of the experimental device, CFD simulations are made respect to the produced one. The simulations are started with RANS method to easily compare the size of the closed environment and propellers. However, RANS solutions have lack of distribution of vortices in the turbulent flow especially which comes from propeller through center of the system. That's why, the generated energy cannot transport to the center.

After selecting nearly size of the experimental box and propellers, LES method is used in CFD simulations with fine grid according to Kolmogorov scale which is calculated from RANS results. By doing that, the vortices can be seen everywhere, and the found down scales are less than the Taylor length scale which is necessary for the research goal. With LES solutions, the RPM value and the distance between propellers can be determined to breakup 2 mm droplet.

In the LES simulations, the turbulent kinetic energy and dissipation rate can not be found in the model. There should be a collected velocity data with probes near the center or the focused volume. These velocity data is processed with analytical approach of turbulent flows. Solving the dissipation rate leads the solution to find D_{max} value.

A novel experimental device is designed as same as in the CFD works. Simplicity of the design has a significant role to achieve coaxial placed propellers and eliminate the errors during manufacturing. In addition, servo motors should be work with in high frequency as 10 hertz to provide wide range of turbulent conditions.

The droplet generator is placed on top of the system and the produced droplets can reach at center of the system where the turbulent quantities are properly settled. A high-speed camera for observing droplet behavior, a hot wire system to measure velocity in the system and a data processing algorithm is prepared to investigate the relation between the droplet and turbulent flow.

1.8 Structure of the Thesis

In the thesis, Chapter 2 explains the numerical and analytical approaches for investigating the turbulent kinetic energy, turbulent dissipation rate, droplet diameter to breakup, length scale of the flow, isotropy and homogeneity to design the wind tunnel. In the Chapter 3, the experimental setups and equipment which are utilized for building wind tunnel, producing droplets and calibrating the hot wire device. The experimental results are displayed and explained in the Chapter 4 with interesting droplet breakup examples and wind measurements. Finally, conclusions are at the end of the thesis as Chapter 5.

CHAPTER II

NUMERICAL AND ANALYTICAL APPROACH

2.1 Numerical Approach

CFD study of the present work includes RANS and LES methods and comparison of different sized test chambers, propellers, and speed of propellers. For basic comparisons and proof of concept, RANS method is used due to its simplicity and low computation time. On the other hand, RANS equation cannot solve vortices because averaged solutions struggles to develop unstable eddies which feed the turbulent energy in the system. However, results from RANS simulations have an impact on decreasing the number of design possibilities and LES application especially in grid size.

Two parameters are important for the correct application of the LES method; grid size and time step. Considering that this method reflects the effect of small eddies on a model flow such as k-eps, increasing the resolution of the grid structure and reducing the cell dimensions will reduce the negative effect of this modeling on the accuracy of the solution. But reducing the size will increase the number of cells to fill the same flow cell and the computational cost will increase considerably. To solve the mentioned optimization problem, first, the Taylor microscale, which derived from the results of the RANS method and calculated to be in the system, should be calculated. In this way, cell sizes of regions that are important to examine can be determined. In addition, considering the drop sizes to be used in the experimental setup, the cell size smaller than this drop size should be in the center. Likewise, high resolution is very important in detailing the environment around the drop while analyzing the results obtained because of the LES simulation analytically.

The Taylor micro scale value is 7.09 mm, and the Kolmogorov scale is 0.2 mm, calculated according to the results of the propeller system with a blade diameter of 100 mm and a length of 100 mm, solved by the time-dependent RANS method in the first report, rotating at 2000 RPM with 400x400x400 mm cube. Since the same RPM value and propellers will be used in the first LES study, the cell size of the lattice structure in the center is 0.5 mm, which is between these two values, even far below the Taylor micro scale. The biggest reason of selection of grids size is that the calculated Taylor microscale is much larger than the planned drop. In addition, the 'Convective Courant Number' value, which is another parameter of the reliability of the CFD study, was determined as ¡1 for all cases and the appropriate time step value was defined to compress it below 1. The simulation performs five internal iterations for each general iteration, and each general iteration advances by 0.00005 sec.

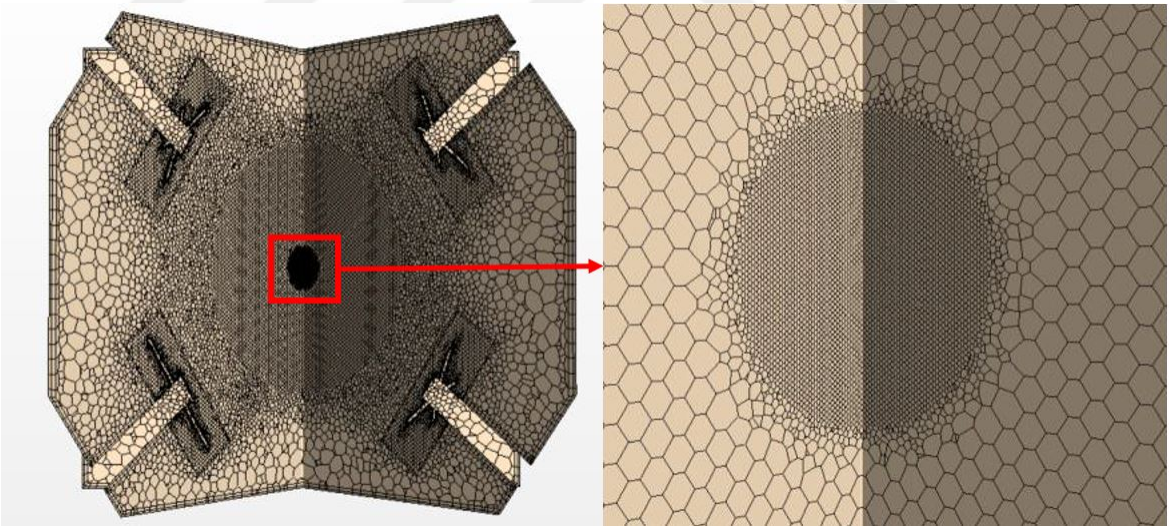

Figure 1: Grid structure of the CFD simulations

The flow environment is already filled with ideal gas and assumed as implicit unsteady and segregated. The properties of air as dynamic viscosity, molecular weight, specific heat, thermal conductivity and turbulent Prandtl number are identified respect to room temperature and atmospheric pressure. The LES method is solved

with WALE subgrid scale. To rotate the propellers, due to computation cost and complexity of actual rotating movement in CFD studies, reference frame model is applied to create a rotating flow without changing the mesh structure. Instant images of velocity vector field from LES simulations can be seen in Figure 2.

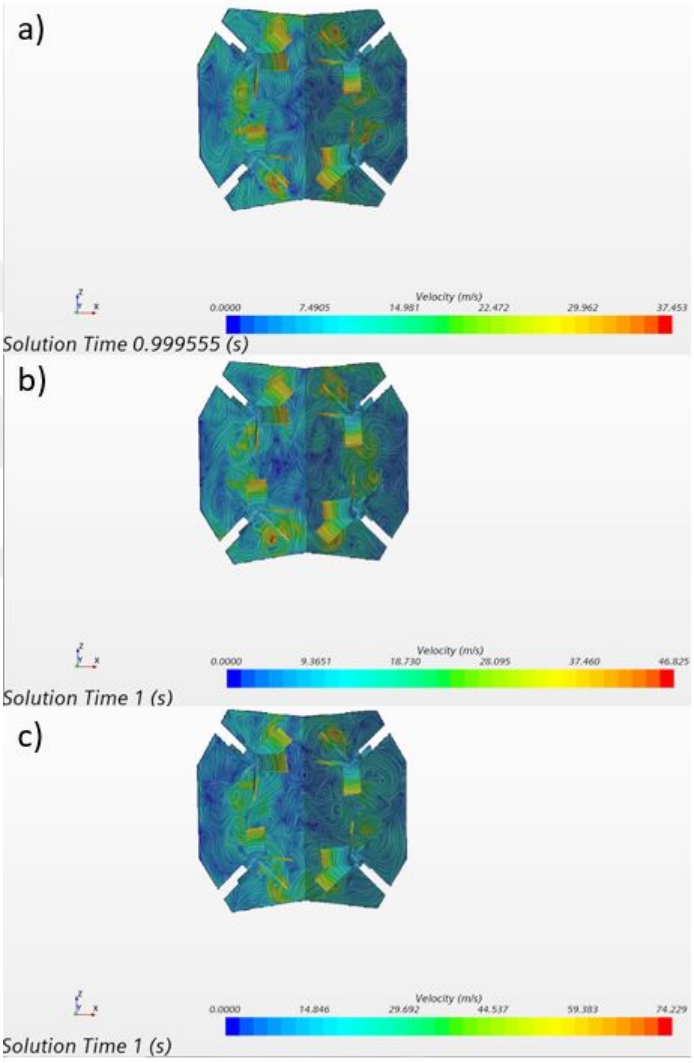

Figure 2: Velocity vector field in 300x300x300 mm cubic test chamber with the propeller speed of a)5000 RPM, b)6000 RPM and c)8000 RPM

As a proof for the concept, the average velocity at the center with 3D components nearly equals to zero. The instantaneous velocity at the center for 5000, 6000 and 8000 RPM is shown in the Figure 3.

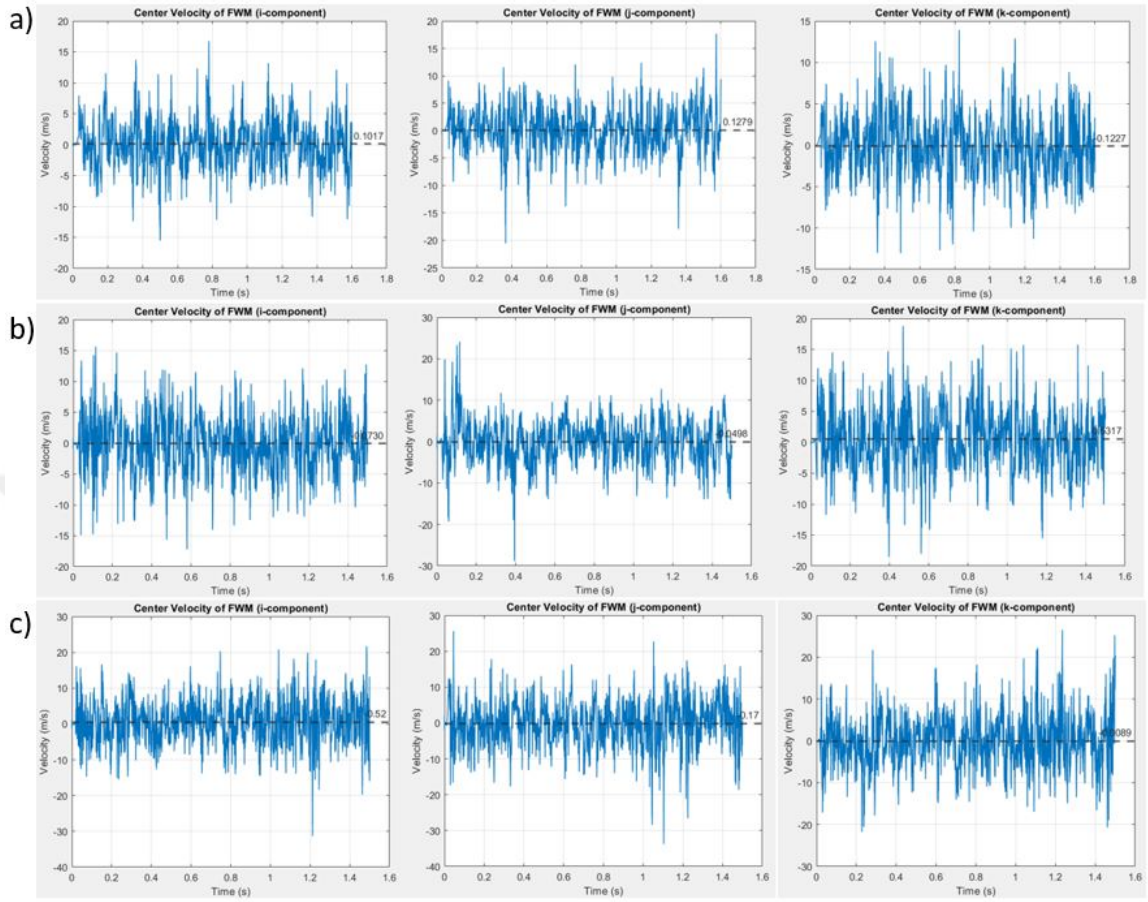

Figure 3: Instantaneous velocity components at center of the 300x300x300 mm cubic test chamber with the propeller speed of a)5000 RPM, b)6000 RPM and c)8000 RPM

2.2 Analytical Approach

Analytical approach of the present study utilizes data from 109 probes with 0.5- and 1-mm displacement as pair of three points by distributing them symmetric along x, y and z-axis between -11.5 and 11.5 mm. The points are placed with same center as the test cell and collect instantaneous vectoral velocity components with magnitudes. Three of the cases in 300x300x300 mm cubic shaped box which are as 5000, 6000 and 8000 RPM cases, are selected to investigate analytically.

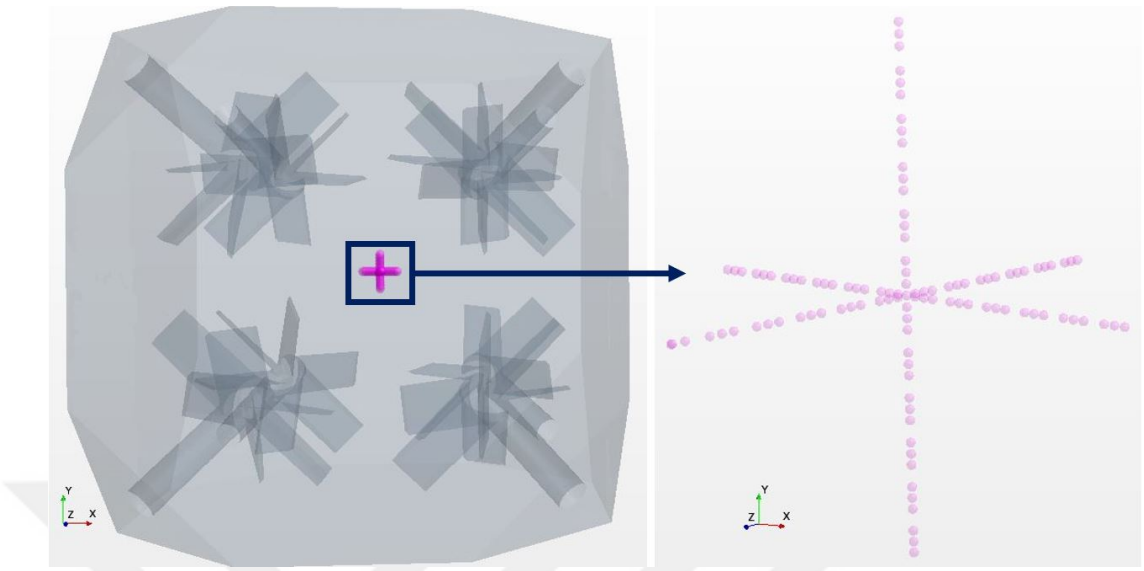

Figure 4: Point probes to collect instantaneous velocity data

2.2.1 Turbulent Kinetic Energy

Energy from the fluctuations which is equal to difference between mean and instantaneous velocity, generates the turbulent kinetic energy (TKE). By using classical kinetic energy formula with fluctuated velocity values instead of velocity magnitude, the turbulent kinetic energy is explained as follows. For 3D space, the components of velocity are combined[18]

$$k = \frac{1}{2}(u_x^{'2} + u_y^{'2} + u_z^{'2}) \tag{10}$$

In addition, power spectrum density of velocity magnitudes at center respect to wavenumber shows the energy in vortices in that wavenumber. By adding the energy of vortices together, the total kinetic energy can be found which equals to area under the curve of the PSD graph.

$$\kappa_{\kappa_a,\kappa_b} = \int_{\kappa_a}^{\kappa_b} E(\kappa) d\kappa \tag{11}$$

The PSD curves are as follows;

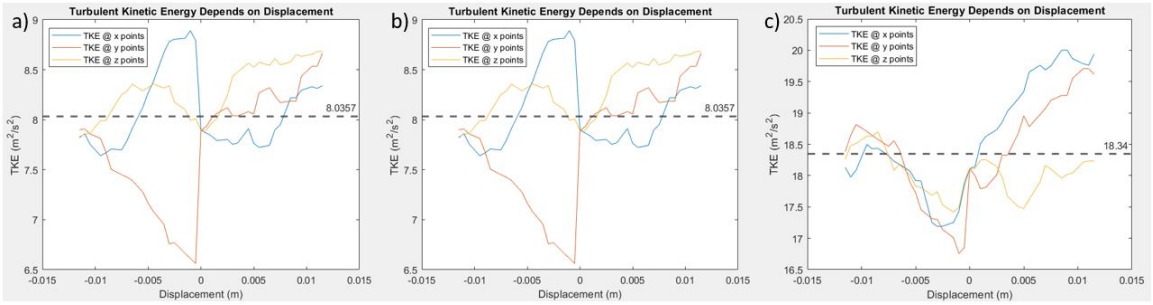

Figure 5: Turbulent kinetic energy in the probes respect to placement of them respect to Eq.10 a)5000 RPM, b)6000 RPM and c)8000 RPM

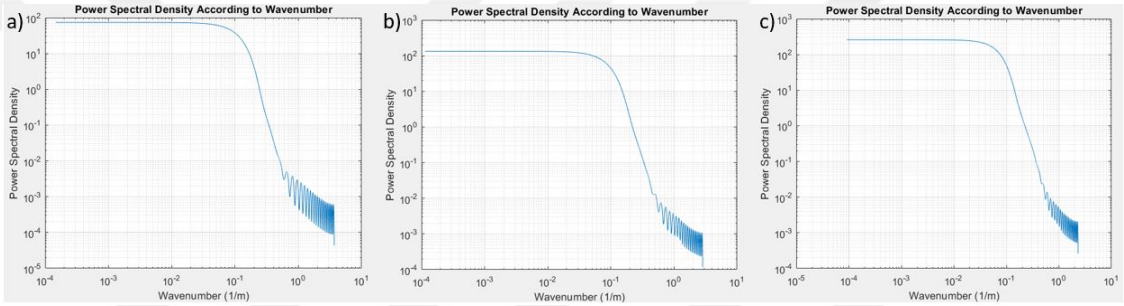

Figure 6: PSD curve of the center probe a)5000 RPM, b)6000 RPM and c)8000 RPM

Adding root mean squared values of velocity fluctuations equal to turbulent kinetic energy as described as in Eq.12 [23].

$$u_{rms,total} = \sqrt{u_{x,rms}^2 + u_{y,rms}^2 + u_{z,rms}^2} = u_{rms,total}^2 \tag{12}$$

The comparison between these three perspectives on calculating the TKE magnitude shows a slight difference between methods due to its isotropic and homogenous nature. In addition, collecting necessary amount of data is a crucial point of chaotic data processing.

Table 9: Comparison of different approaches about TKE calculation

	Turbulent Kinetic Energy (m^2/s^2)					
Rotational Speed (RPM)	From PSD (Eq.11)	From RMS (Eq.12)	From ins. vel. fluc. (Eq.10)			
	Total TKE	Total TKE	Total TKE	TKE on x-axis	TKE on y-axis	TKE on z-axis
5000	7.8798	7.8955	8.0357	8.0759	7.7451	8.2861
6000	11.2959	11.3017	11.5051	11.2854	11.8187	11.4112
8000	18.0567	18.1127	18.3437	18.1127	18.3733	18.0325

2.2.2 Turbulent Dissipation Rate

The dissipation rate (TDR) can be derived from the same power spectrum by manipulating the spectrum with kinematic viscosity and wavenumber inside the integral. The same PSD as in TKE is utilized to find TDR [18].

$$\epsilon_{\kappa_a,\kappa_b} = \int_{\kappa_a}^{\kappa_b} 2\nu\kappa^2 E(\kappa) d\kappa \tag{13}$$

On other hand, the definition of turbulent dissipation rate is the transferred energy from large eddies to smaller eddies. Large eddies feed from the generated momentum from any source but if the source is stopped, large eddies start to fade out and divided into smaller pieces with its energy. For the present study, the stopping of the propellers and the energy loading of the flow is ended and the process of energy cascading starts. The change in turbulent kinetic energy in the flow starts to decrease due to cascading phenomenon. Although this energy transfer describes the basic definition of the dispersion rate, the change of turbulent energy depending on time will be equal to the dispersion rate [18].

$$\frac{dk}{dt} = -\epsilon \tag{14}$$

Central differencing method is used for derivation operation. The turbulent kinetic energy magnitudes are taken from the solution of Eq.12. The sudden changes in the graph shows the dissipation in forced turbulence with propellers.

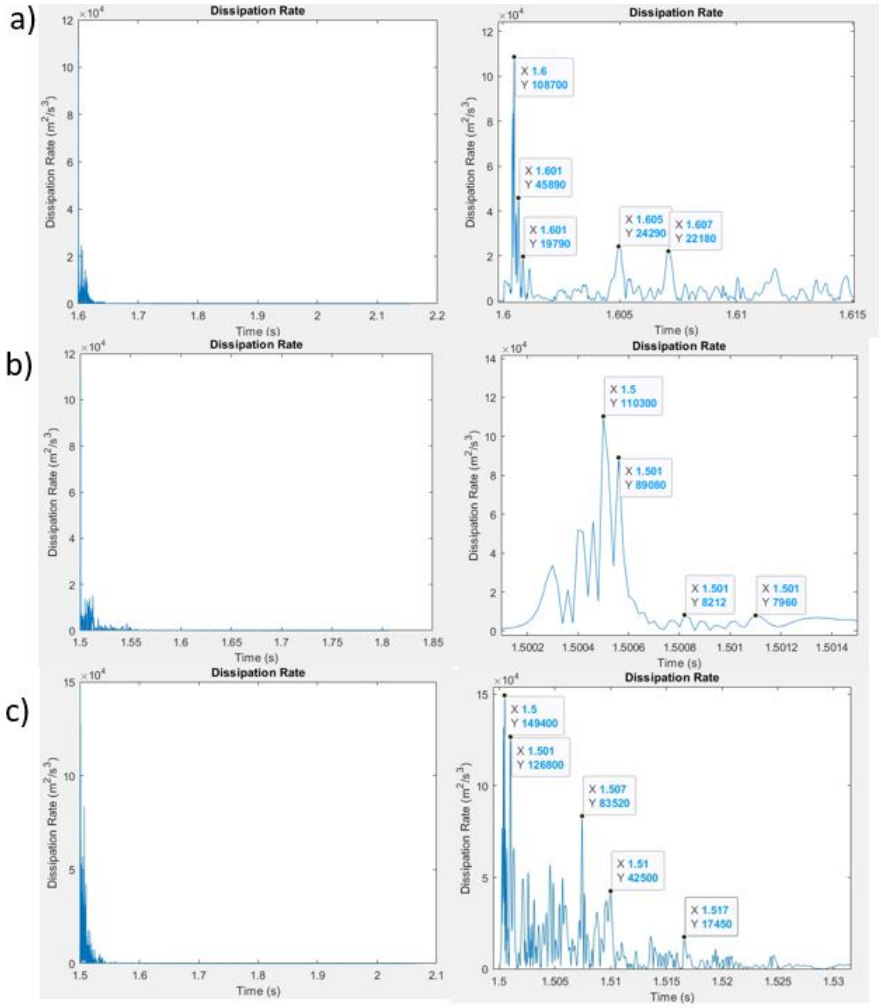

Figure 7: Turbulent dissipation rate of the three cases; a)5000 RPM, b)6000 RPM and c)8000 RPM

Table 10: Comparison of different approaches about TDR calculation

	Turbulent Dissipation Rate (m^2/s^3)	
Rotational Speed (RPM)	From Eq.13 (PSD)	From Eq.14 (dk/dt)
5000	14291	21350
6000	11051	20560
8000	14533	13960

2.2.3 D_{max} Values

The equation of Hinze's work (Eq.4) is used to determine the biggest unbreakable droplet diameter for three cases according to found dissipation rate with derivative of kinetic energy respect to time. Ethanol and water droplets are investigated.

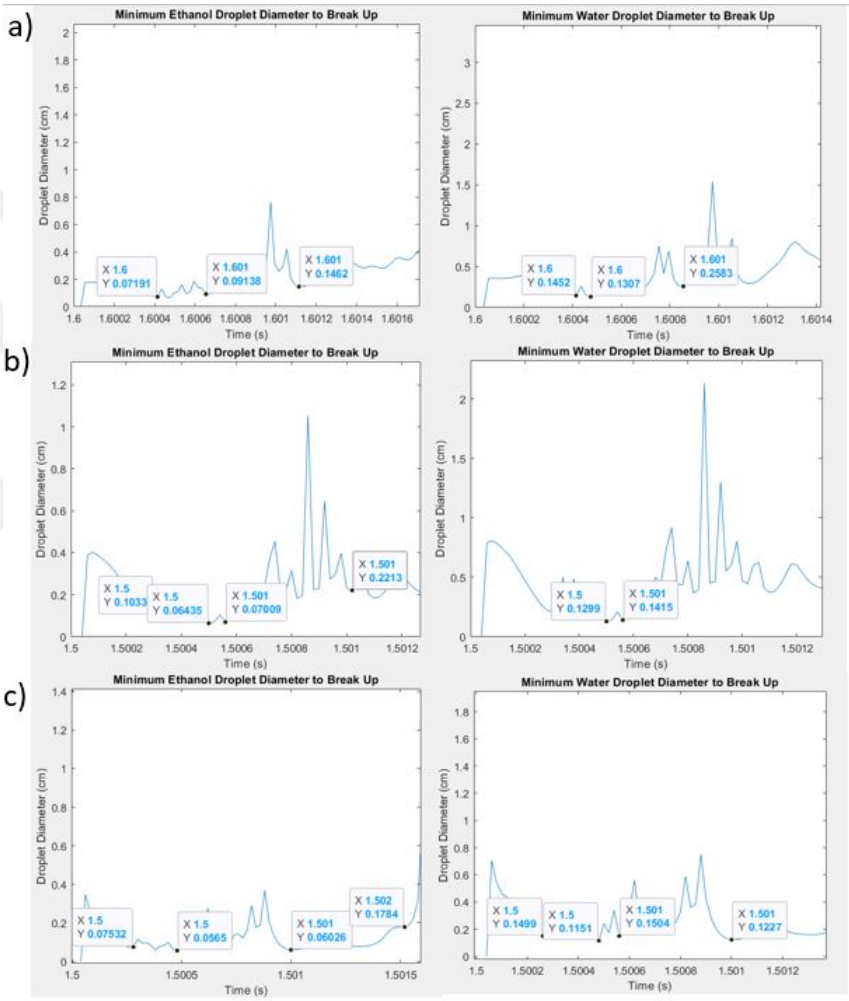

Figure 8: D_{max} values of the cases; a)5000 RPM, b)6000 RPM and c)8000 RPM

Table 11: Comparison of simulation results with changing in the RPM value and D_{max} results

Model specification	$\varepsilon(m^2/s^3)$	D_{max} for water(cm)	D_{max} for ethanol(cm)
300 mm, 120 mm propeller diameter, 5000 RPM	21350	0.252	0.123
300 mm, 120 mm propeller diameter, 6000 RPM	20560	0.256	0.125
300 mm, 120 mm propeller diameter, 8000 RPM	13960	0.299	0.149

Considering the results obtained, the targeted results for the experiment were achieved. All three systems are capable of breaking up small ethanol drops within 2 mm. In addition, the LES method is the best method in the process of transferring the flow generated by the propeller to the center, but it has still errors when compared with DNS. It is thought that a water drop with a diameter of 2 mm can also be broke up in the test chamber.

2.2.4 Two-point Correlation

Two-point correlation was introduced by von Karman and Howarth as a result of his work on the statistical theory of turbulence[24]. This study is based on the generation of two separate functions by using the oscillation velocity values that are perpendicular and parallel to the position vector at two different points selected in the flow. The difference between two points should be used as a constant for all correlations as 'r = x1 = x2'. According to whether the velocity components are parallel or perpendicular, two separate correlation functions are indicated as 'f' and 'g'. For the two-dimensional plane, the following correlation functions define 'f' and 'g' Direction of the velocity component and selected axis are used in 'f' and 'g' functions, are explained more clearly in Figure 9 on the two-point correlation plot for isotropic turbulence. The specified equations of the correlation functions in another axis and component are observed when turbulence is the isotropic condition of the flow.

These functions show the correlation between two points of fluctuation velocity

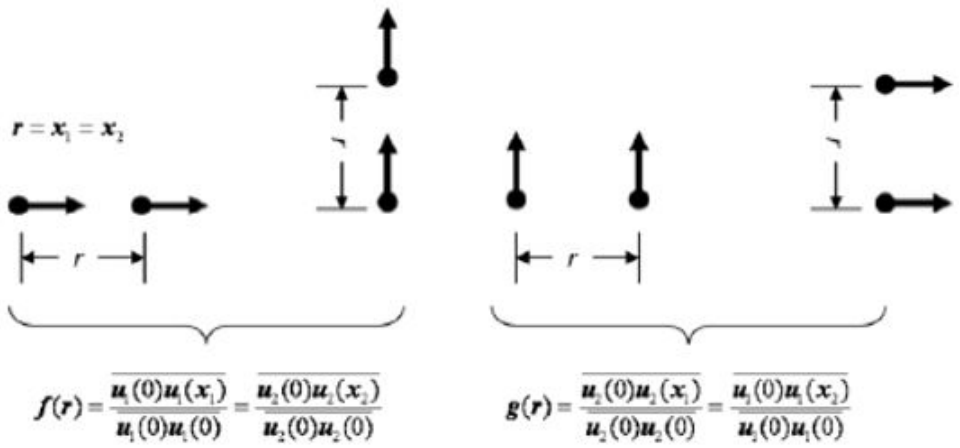

Figure 9: Two point correlation for isotropic turbulence

values indicating the turbulent properties of the flow. As the distance between the points, 'r', increases, the correlation value should decrease. The distance between them should be determined according to the sensitivity desired to be examined. In addition, the calculated correlation functions can be used to determine the dissipation and integral length scale measures. Also, the equality in two dimension due to isotropy can be expanded to third (z-axis) dimension. From isotropy assumption

$$f(r) = \frac{\bar{u_1(0)}u_1(x_1)}{\bar{u_1(0)}u_1(x_0)} = \frac{\bar{u_2(0)}u_1(x_2)}{\bar{u_2(0)}u_2(x_0)} = \frac{\bar{u_3(0)}u_3(x_3)}{\bar{u_3(0)}u_3(x_0)} \tag{15}$$

$$g(r) = \frac{\bar{u_2(0)}u_2(x_2)}{\bar{u_1(0)}u_1(x_2)} = \frac{\bar{u_2(0)}u_1(x_2)}{\bar{u_2(0)}u_2(x_0)} = \frac{\bar{u_3(0)}u_3(x_3)}{\bar{u_3(0)}u_3(x_0)} \tag{16}$$

Approximately 110000 velocity values were recorded for the components of the speed value at each point on each axis by running the CFD study in real time with 2.15 seconds, 0.00001 seconds during the operation of the propellers, and 0.00002 seconds when stopped. In the whole study, approximately 24 million pieces of velocity data are used for each correlation. In the study of chaotic processes, the specified amount of data is collected, because increasing the data density has allowed the results to be more reliable.

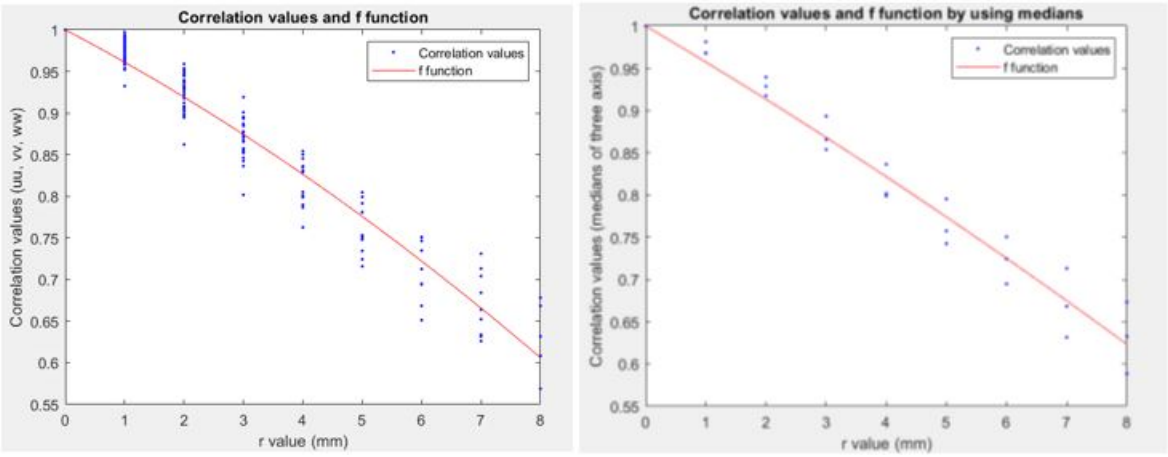

Figure 10: Two-point correlation for 5000 RPM. In left, whole data from all probes is used. In right, the data is averaged respect to its position axis

In the study, there is a data manipulation process because the correlation with a lower 'r' amount has more data and the median of all three axes which bends the curve of the first correlation being 1 by its definition. Therefore, while calculating the 'f' and 'g' functions, the medians for all axes are calculated and the graphs below are drawn for each CFD study. Since there is a maximum difference of 2.11 percent between the equations the 'f' and 'g' functions, which displays high isotropy in the flow, the median values could be used in the calculations. At the same time, this low difference supports the isotropic nature of the flow.

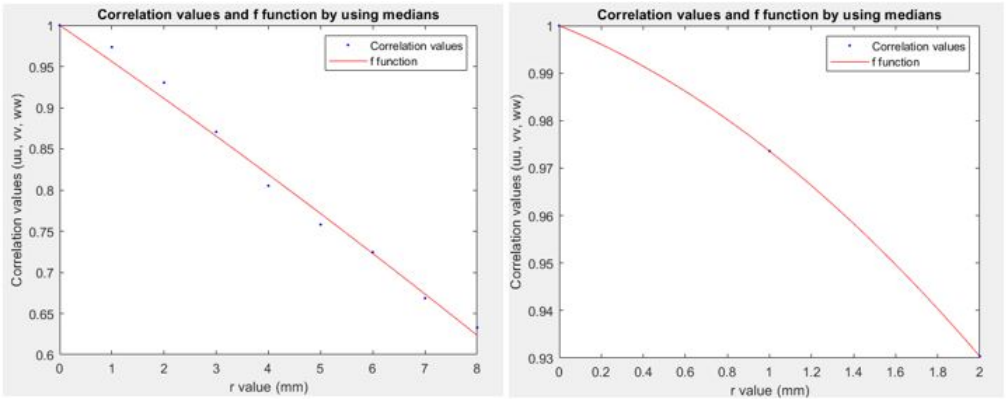

Figure 11: Two-point correlation for 5000 RPM with 'f' function. The left graph include all 'r' values.The right graphs use the average value.

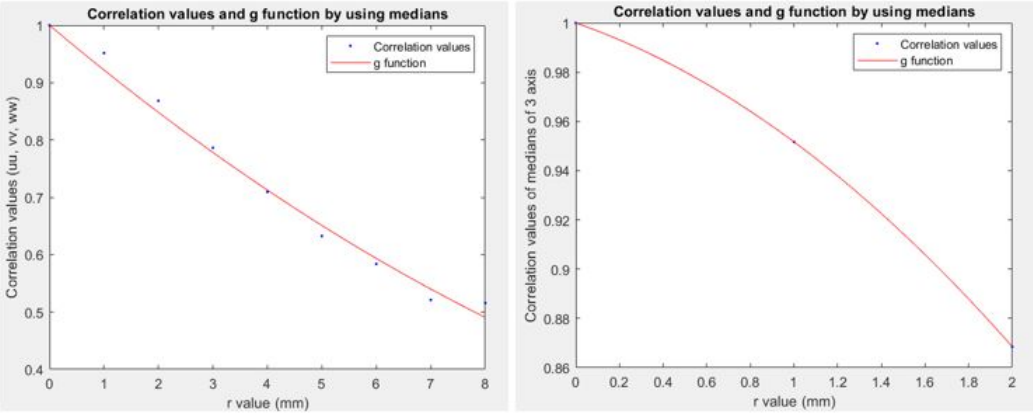

Figure 12: Two-point correlation for 5000 RPM with 'g' function. The left graph include all 'r' values.The right graphs use the average value.

According to these three cases, the two point correlation is investigated with averaged curve, left ones in the figures above, and a parabolic function to find the value of intercepting point on x-axis to find Taylor microscale which also shows the end of the correlation. The described method is applied for other experiments. The comparison of them can be seen in Table 12.

Table 12: Taylor microscale results respect to RPM value of the propellers

	5000 RPM	6000 RPM	8000 RPM
λ_f	9.8895	8.1472	9.4294
λ_g	6.7417	6.8361	6.6997

2.2.5 Isotropy and Homogeneity of the Flow

It is crucial to test the isotropy state of the system through the calculation of anisotropic tensor and invariants of the turbulent flow. In order to ensure about the assumptions made in the analytical and numerical approach, the isotropy state of the flow must be questioned. The first step to determine the level of isotropy of the flow is to calculate the dimensionless anisotropic tensor. This can be achieved by utilizing the relation:

$$a_{ij} = \frac{\overline{u_i u_j}}{2k} - \frac{1}{3}\delta_{ij}, \quad \text{where if } i = j \rightarrow \delta_{ij} = 1; i \neq j \rightarrow \delta_{ij} = 0 \tag{17}$$

In which $\overline{u_l u_j}$ is the averaged Reynolds stresses k is the turbulent kinetic energy and δ_{ij} is Kronecker delta. This relation is simply the ratio between Reynolds stresses and kinetic energy of the flow. Utilizing this tensor, one can calculate the invariants of the flow to compare the results by looking at a map introduced by Lumley; Lumley Invariant map (seen in Figure 13), also known as anisotropy invariant map (AIM) [6]. The invariant map is a great tool to determine the characteristic states of turbulence such as the level of isotropy and axisymmetry of the flow.

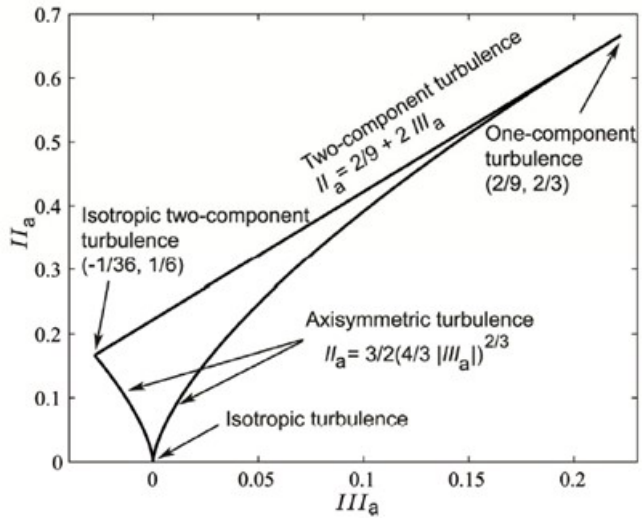

Figure 13: Anisotropy invariant map from the work of Lumley [6]

The eigenvector of the anisotropy tensor must be calculated by diagonalizing the anisotropy tensor and finding the eigenvalues.

$$\widehat{a_{ij}} = \begin{bmatrix} \lambda_1 & 0 & 0 \\ 0 & \lambda_2 & 0 \\ 0 & 0 & \lambda_3 \end{bmatrix} \tag{18}$$

λ_i are the eigenvalues of the anisotropy tensor. The first, second, and third invariants can be found by utilizing the eigenvector of the anisotropy tensor.

$$
\begin{aligned}
I_1 &= \mathrm{tr}\left(\widehat{a_{tj}}\right) \\
I_2 &= \frac{1}{2}\left(\mathrm{tr}\left(\widehat{a_{ij}}\right)^2 - \mathrm{tr}\left(\widehat{a_{tj}}^2\right)\right) \\
I_3 &= \det\left(\widehat{a_{ij}}\right)
\end{aligned}
\tag{19}
$$

The invariants II and III must be calculated to be able to figure out the coordinates on the anisotropy invariant map. These variables can be found through the relations below.

$$
\begin{aligned}
II &= -2I_2 \\
III &= 3I_3
\end{aligned}
\tag{20}
$$

The result of these calculation indicates that the flow is highly isotropic. The calculations were done for the 109 probes as specified in the numerical part as in Figure 14 from which the velocity data were extracted while conducting the simulations. Whole invariant values from the points are in the region of isotropic turbulence. However, as it can been that in Figure 14, increasing the speed of the propellers creates more isotropic flow. In addition, for 5000 RPM, the invariants are nearby to left curve which improves the chance of axisymmetric turbulence. The results can be seen from the figure below.

On the other hand, the invariances of the flow can be investigated by using the ratio of the local RMS velocities on probes placed on three dimensions [18]. For example, the isotropy ratio is defined for 'i' and 'j' velocity components on each probe to divide them separately for each probe and same process works for other dimensions. The ratio of local RMS values

$$
\begin{aligned}
I_{i-j}\left(x_1, x_2\right) &= u_{i,\mathrm{rms}}\left(x_1, x_2\right) / u_{j,\mathrm{rms}}\left(x_1, x_2\right) \\
I_{i-k}\left(x_1, x_2\right) &= u_{i,\mathrm{rms}}\left(x_1, x_2\right) / u_{k,\mathrm{rms}}\left(x_1, x_2\right) \\
I_{j-k}\left(x_1, x_2\right) &= u_{j,\mathrm{rms}}\left(x_1, x_2\right) / u_{k,\mathrm{rms}}\left(x_1, x_2\right)
\end{aligned}
\tag{21}
$$

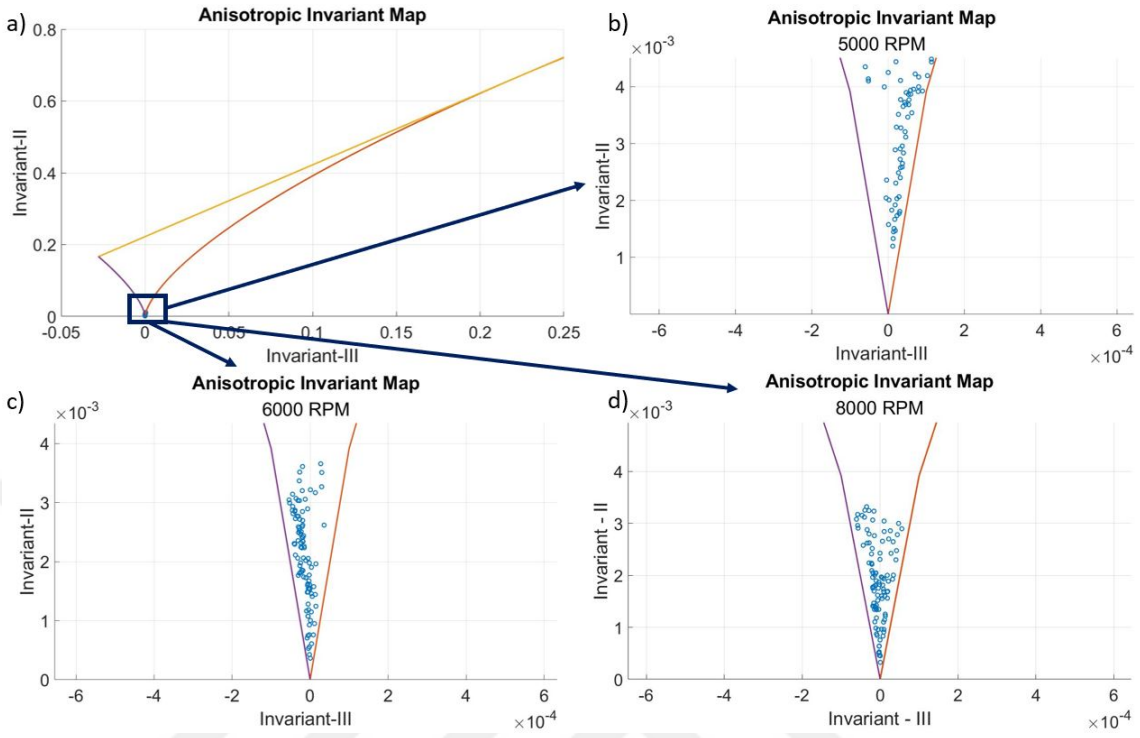

Figure 14: Anisotropy invariant map and results; a) Created AIM for whole regimes, b) AIM for 5000 RPM, c) AIM for 6000 RPM, d) AIM for 8000 RPM

In homogeneous turbulence, the flow field is statistically independent of the change in the coordinate system. A ratio of the local RMS velocity to spatially (3D spaced) averaged RMS velocity identifies the homogeneity which shows the uniformity of the velocity field.

$$\begin{aligned} H_{\mathrm{i}}\left(x_1, x_2\right) &= u_{\mathrm{i,rms}}\left(x_1, x_2\right) / \overline{u_{\mathrm{rms}}\left(x_1, x_2\right)} \\ H_{\mathrm{j}}\left(x_1, x_2\right) &= u_{\mathrm{j,rms}}\left(x_1, x_2\right) / \overline{u_{\mathrm{rms}}\left(x_1, x_2\right)} \\ H_{\mathrm{k}}\left(x_1, x_2\right) &= u_{\mathrm{k,rms}}\left(x_1, x_2\right) / \overline{u_{\mathrm{rms}}\left(x_1, x_2\right)} \end{aligned} \tag{22}$$

These ratios must be equal to one as unity to claimed that the flow is homogenous isotropic flow. The values of the ratios can be seen in Figure 15-16. The invariance and homogeneity functions are approximately unity with small deviations. The provided flow in the numerical work can be defined as homogenous isotropic flow due to this

knowledge.

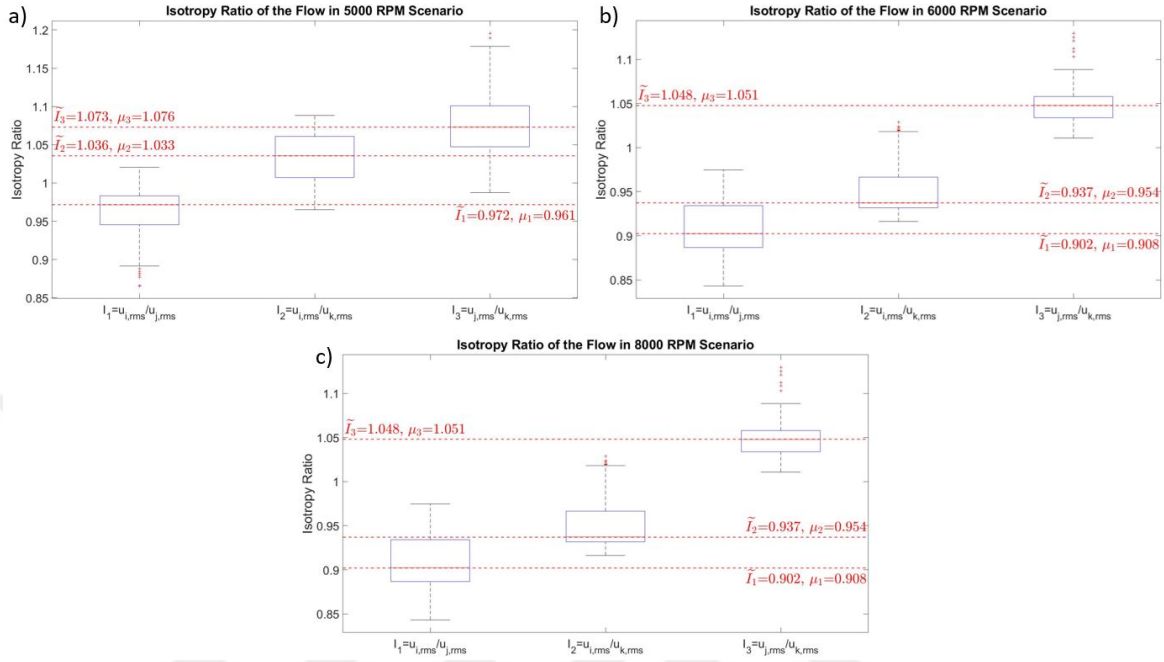

Figure 15: Isotropy ratio of the 109 data probes; a) 5000 RPM, b) 6000 RPM, c) 8000 RPM

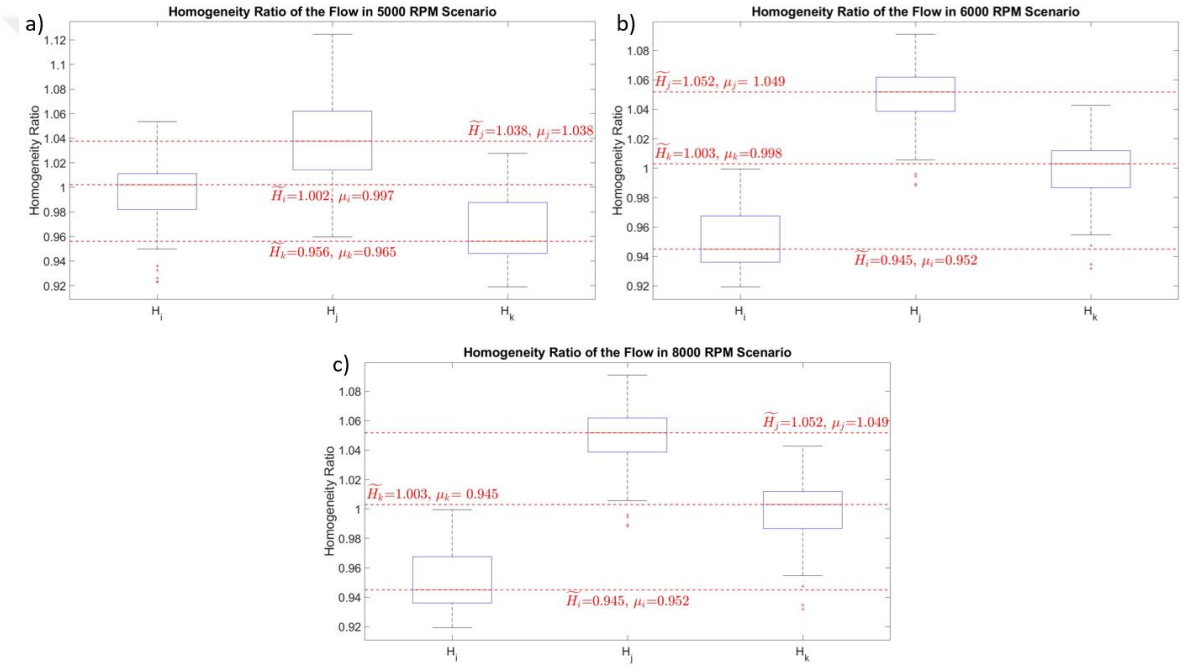

Figure 16: Homogenity ratio of the 109 data probes; a) 5000 RPM, b) 6000 RPM, c) 8000 RPM

CHAPTER III

EXPERIMENTAL FACILITIES

3.1 Design of the Wind Tunnel

Design of the test cell must be similar as in the CFD studies. Therefore, eight propellers should be concentric, and the inner dimensions equals to the cube in 300x300x300 mm. Due to limited budget with the need of excellence, the cubic shape designed as separated in eight corner cubes and twelve rectangular edges. 80x80x80 mm solid aluminum cubes are designed for each corner for the surface required for the assembly of the engine and moving components. To direct the propellers at the center and each other, the outer surfaces of these cubes are shaved with the degree of 45 on outer surface. In addition, the inner surface must be shaved to be placed on the production bench in order to drill holes, both surfaces are shaved 35 mm towards the center of the cube at an angle of 45 degrees. For the assembly of the parts, 20x20x20 mm male connection extensions are made on the side parts and 20x20x20 mm female holes are drilled on the corners. The connection extensions are fixed to the small cubes by using two screws for each connection area. 4 holes will be drilled on the triangular outer surface of the corner cubes. The hole in the center of the triangular surface is drilled with a medium tight fit tolerance and the SKF 2200 ETN9 bearing is inserted as a tight fit and the shaft of the propeller is passed through it.

For the 12 sides of the cube, 40x40x190 mm solid aluminum square prisms are produced. A 20x20x20 mm cube protrusion is formed by trimming the two sides of the side profiles, and two holes is drilled for the screw to be mounted with the corner cubes. In order for the side surfaces of the test cell to be closed with a seal cover or glass, the side parts must have frames. Plates of 5x30x150 mm are mounted on

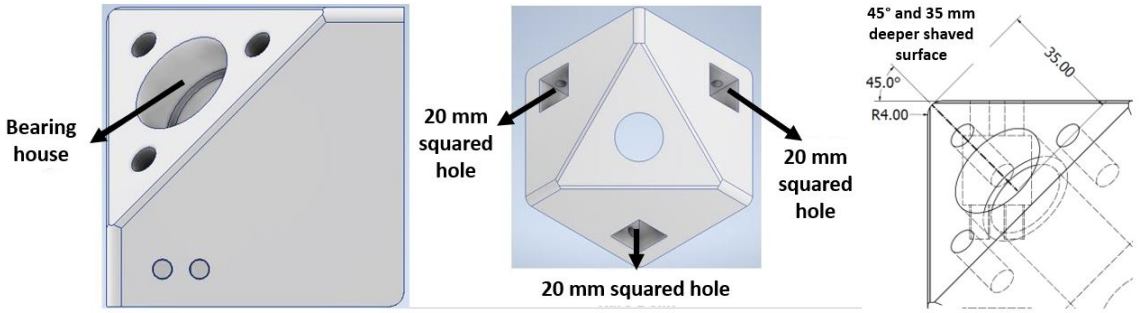

Figure 17: Corner cubes of the wind tunnel

the side profiles as a frame. To fit the frame, 5.5x10 mm channels are opened on one side for the side profiles for those facing the bottom surface and on both sides of those facing the other surfaces. The specified rectangular plates are placed in these channels and the seal covers and glass surfaces are placed on them.

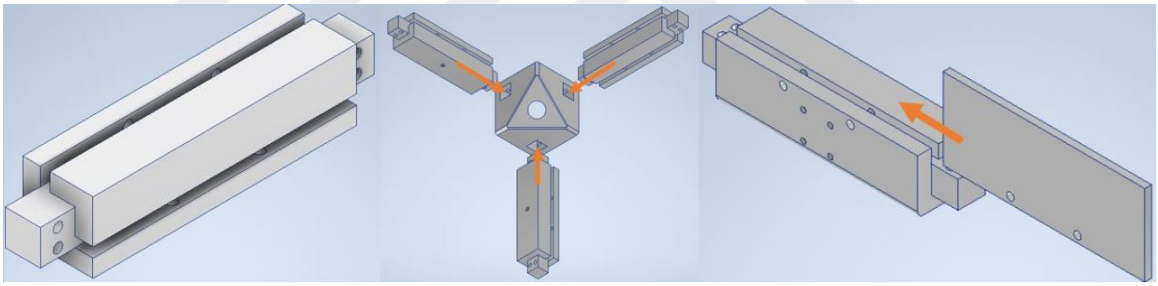

Figure 18: Side profiles and assembly manual

The skeleton of the isotropic turbulent flow tunnel is established as a result of assembling the corner cubes, edge profiles and frames to each other. In this system, the distance between the outer surfaces of the frames where the opposing doors or glasses, is 300 mm. Three side of the test cell has metal covers placed on EPDM sponge for sealing, and other three sides has glasses on with O-rings. The viewing aperture is at least 150x150 mm.

Motor and moving parts are mounted on the triangular surfaces of the corner cubes. The moving system includes 400-Watt Inovance ISMH1 model servo motor, R+W BKC 15 model coupling, two square prism plates of 120x120x10 mm, 4 spacer

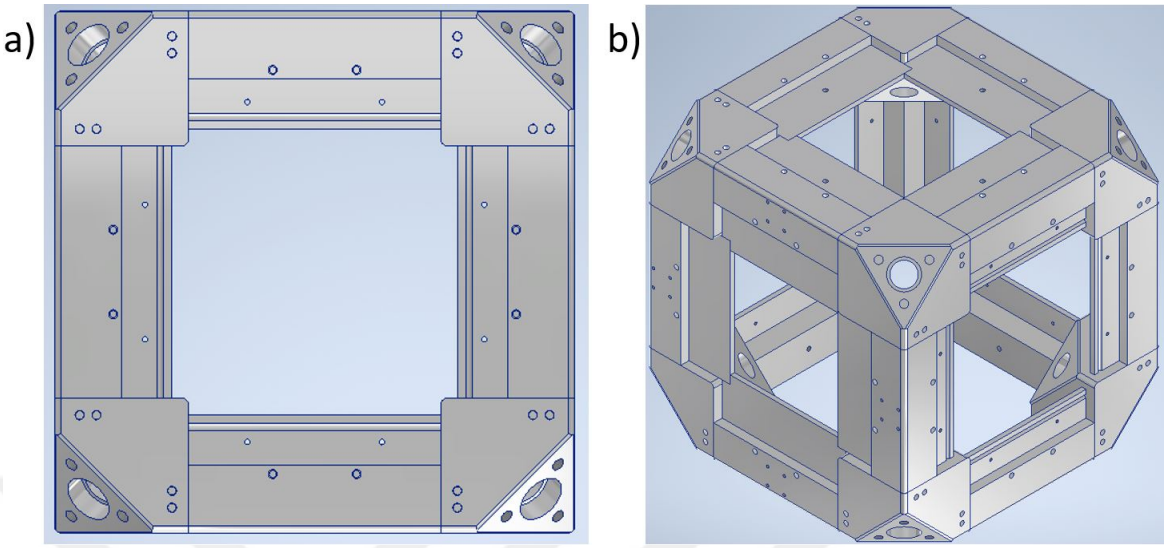

Figure 19: Skeleton of the wind tunnel; a) Front view, b) Isometric view

pipe profiles, propeller, and shaft. The servo motors are fixed to the upper square prism plates which is mounted on lower one with four screws in spacer pipes. A coupling is placed in the gap between the two plates and the movement transfer between the motor and the propeller shaft is provided. The assembly direction and placement of the parts is as in the Figure 19.

The upper, lower and one side surfaces of the cube skeleton of the isotropic turbulent flow tunnel are covered with aluminum covers, and the remaining 3 surfaces are covered using glass. The size of the glass surfaces consists of 220x220 mm squares with cuttings of 40x40 mm from the four corners. The aluminum cover, which is on the side of the system, is designed as hinged, allowing access to the inside of the system. Four flat-bottomed locks (Kukamet 111-L) will be used to ensure sealing by compressing the EPDM sponge on which the side cover is placed. A hard plastic holder is placed on the cover to take it out. Since the aluminum cover, which will be on the upper side, will rarely be opened, it is fixed to the frames with screws to ensure that the EPDM sponge is compressed and sealed. At the center of this cover, a hole is drilled to place a plexiglass tube with inner diameter of 8 mm which protects to

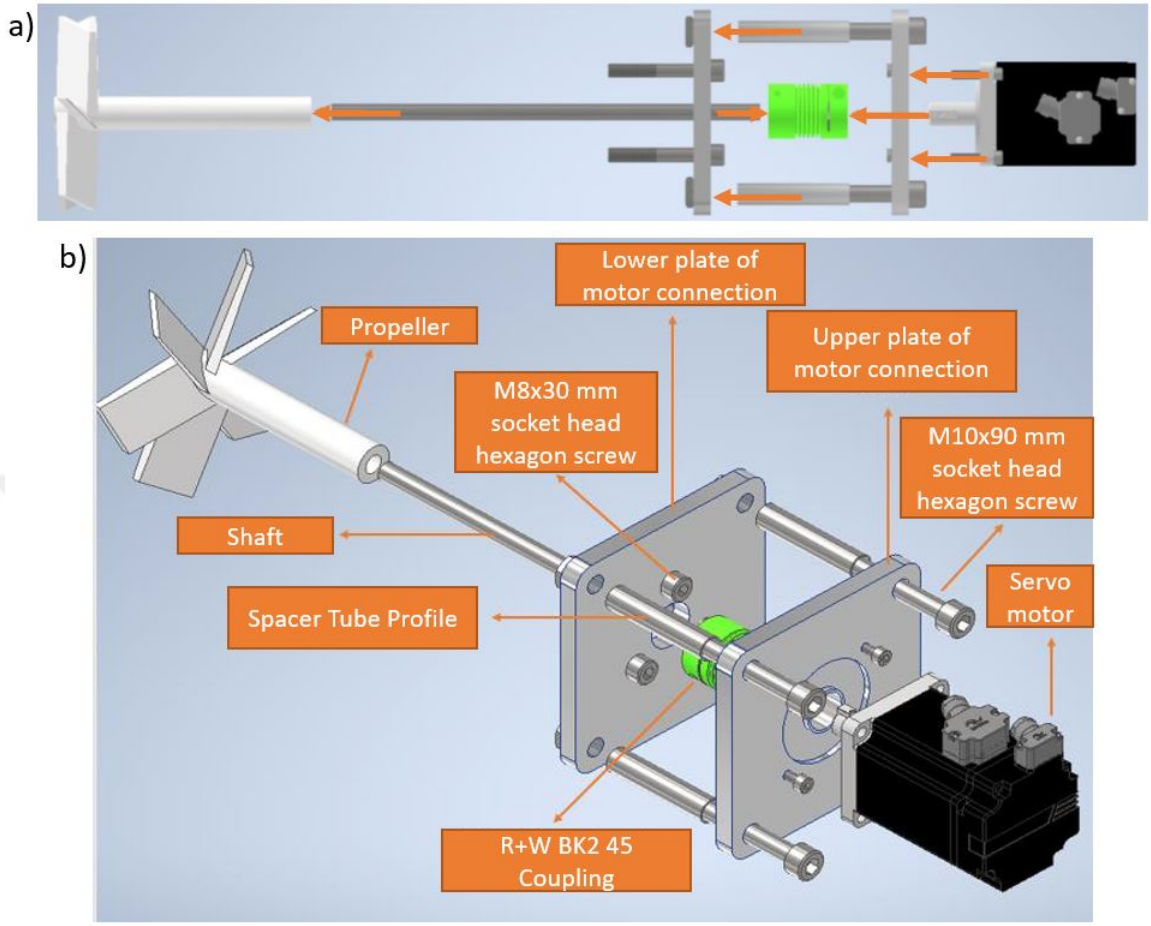

Figure 20: Connection between servo motor and propeller; a) Schematic of the assembly of moving parts, b) Parts of the assembly

droplet until reaching to center of the test chamber. An adjustable holder is found to change the dimension of the plexiglass tube. The bottom cover will be connected to the edge profiles using four aluminum corner connections and the small gap between them will be covered with impermeable silicone. The remaining three surfaces are covered with glass.

In order to operate and observe the system, four pieces of 30x90 mm aluminum sigma profiles, which can be placed on the optical table and ensured to stand, are used by cutting 200 mm in length. The stress analyzes of these profiles, which should carry the whole system, were made within the Inventor program and the measurements is

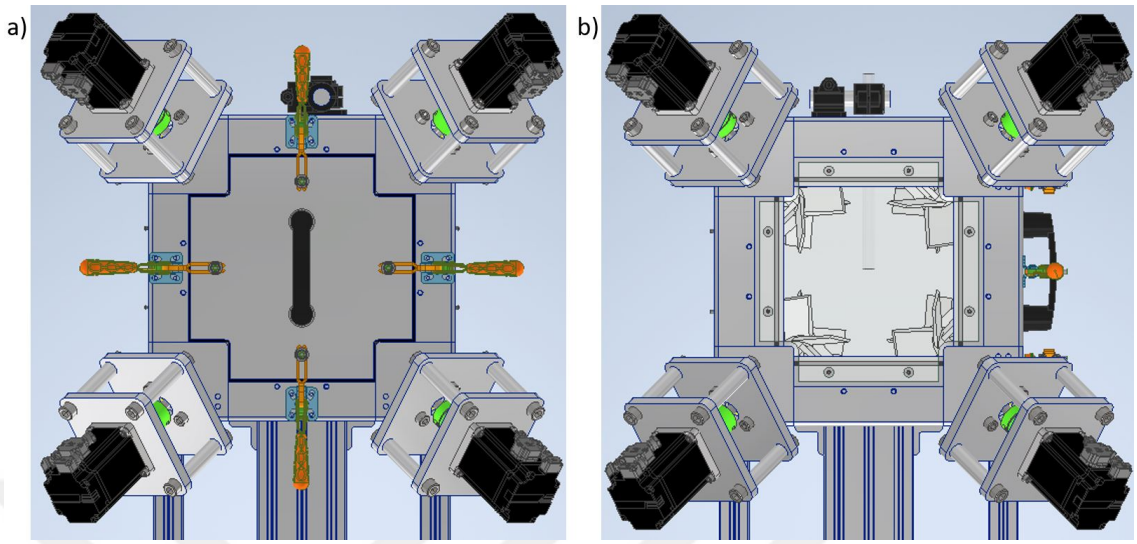

Figure 21: Isotropic turbulent flow wind tunnel design in CAD environment; a) Front view, b) Side view

found applicable. The sigma profiles are mounted to the edge profiles in the cube frame with 30x30 mm aluminum corner connection. Side profiles are fixed with two narrower surfaces of each sigma profile. The bottom surfaces of sigma profiles are fixed to the optical table using 90x90 wide corner joint. As a result of this settlement, the assembly of the whole system is completed, and it is ready for testing. The manufactured and assembled experimental system can be seen in Figure 22.

3.2 Droplet Generation

A syringe pump is used to produced droplets with the size of nearly 2 mm in diameter. By changing the mass flow rate the syringe, the velocity and time scale of the droplet generation increases. The syringe needle is placed at the end of the plexiglass tube due to avoid the acceleration caused by gravity. The produced droplets are observed and measured with a high-speed camera.

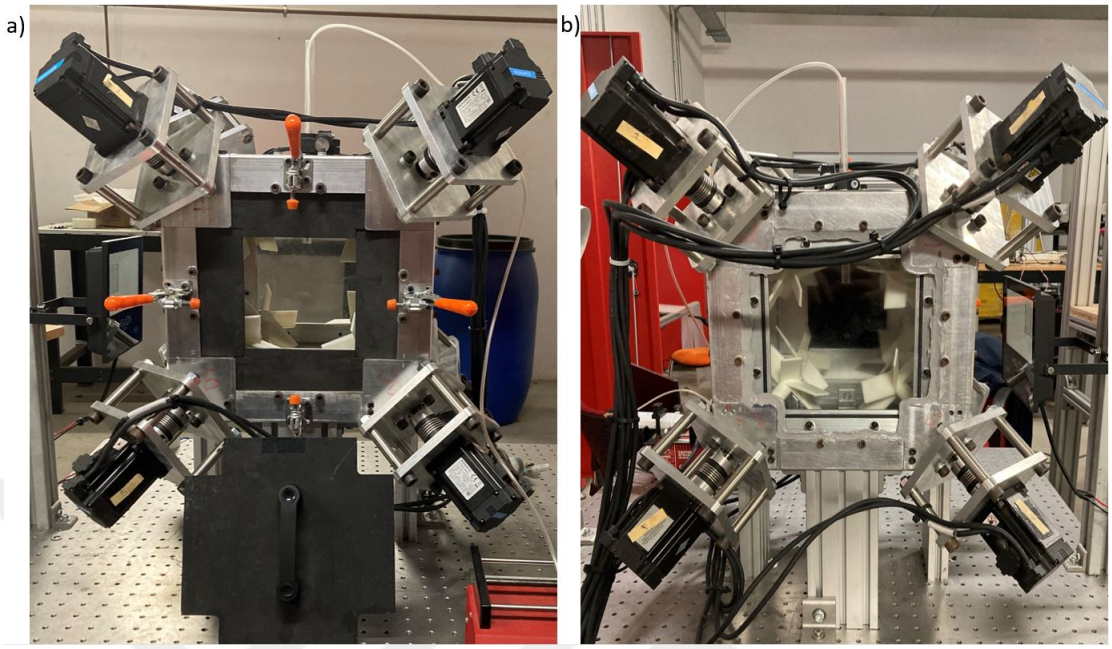

Figure 22: Isotropic turbulent flow wind tunnel; a) Front view, b) Side view

3.3 Calibration Setup for the Hot-wire Experiments

Velocity calibration of the hot wire probe employed in a test section as shown in Figure 24. The test section includes a 12V computer fan, honeycomb grid with hexagons with sides of 1 cm, a PVC tube with inner diameter of 12 cm and a nozzle by reducing the diameter to half of the PVC tube. A pressure transducer of ABB 266DSH and a NI DAQ system were utilized to collect the data to observe the relation between velocity of the flow and voltage response of the hot-wire probe.

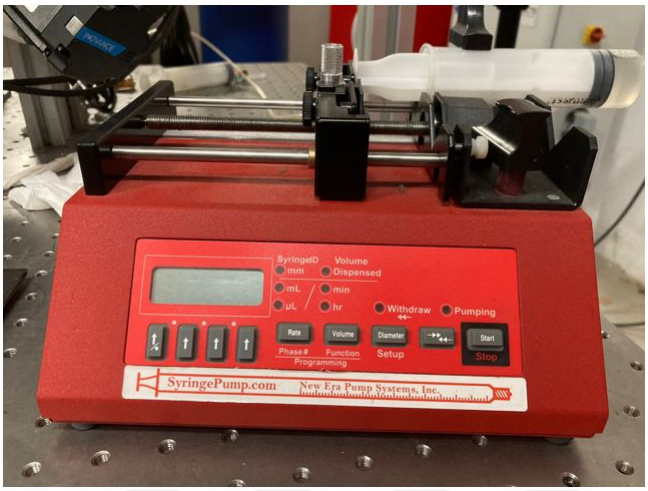

Figure 23: Syringe Pump

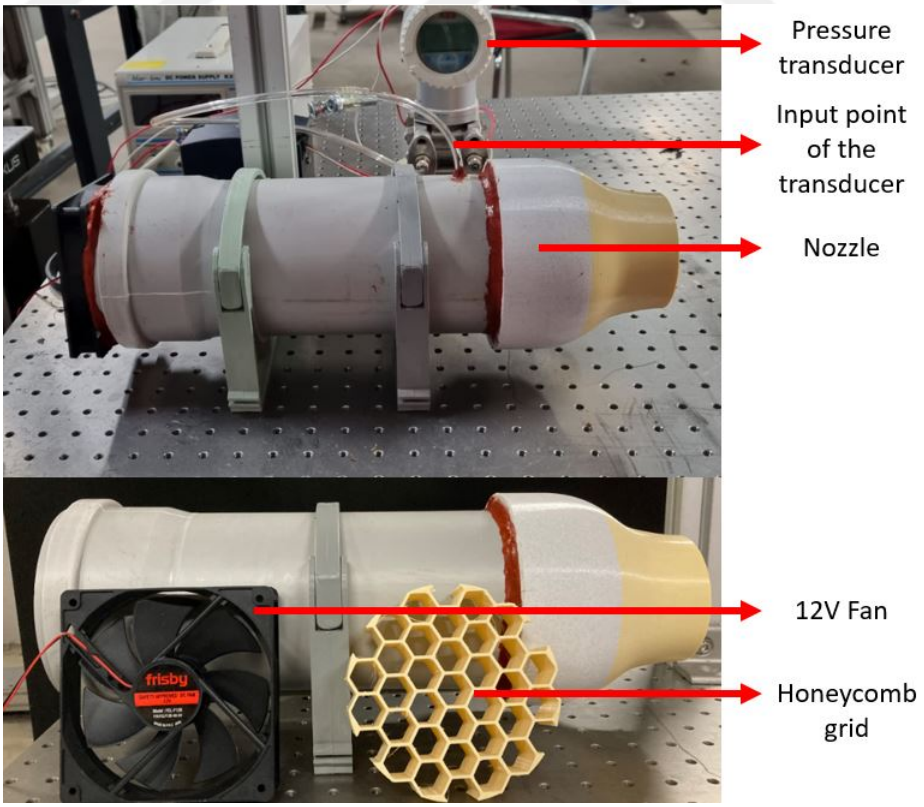

Figure 24: Test section for calibration process of the hot-wire system

CHAPTER IV

EXPERIMENTAL RESULTS

4.1 Droplet Breakup in the Wind Tunnel

The servo motors can run various velocity profiles limited by 10 hertz for data processing. The velocity profiles are built in Excel and imported into control unit. In whole scenarios, same velocity profiles are given into each servo motor to push the air forward. To test the droplet breakup capability of test cell, experiments are started by speeding the propellers to 2000 RPM. However, droplet breakup does not occur during these tests. Between the speed of 2500-6000 RPM, droplets can breakup with different counts and probabilities in various breakup types. Count of the produced droplets are changed between 10-15 due to wind condition and caught frames in 1.7 sec. However, the measurement is started after minimum 5 sec after reaching the wanted RPM magnitude by adding 50 RPM at each time step. In addition, two different sine function with two different hertz are built between 5000-6000 RPM to create more randomness for stronger turbulence. The waited time of starting measurements is 10 sec for sine applications.

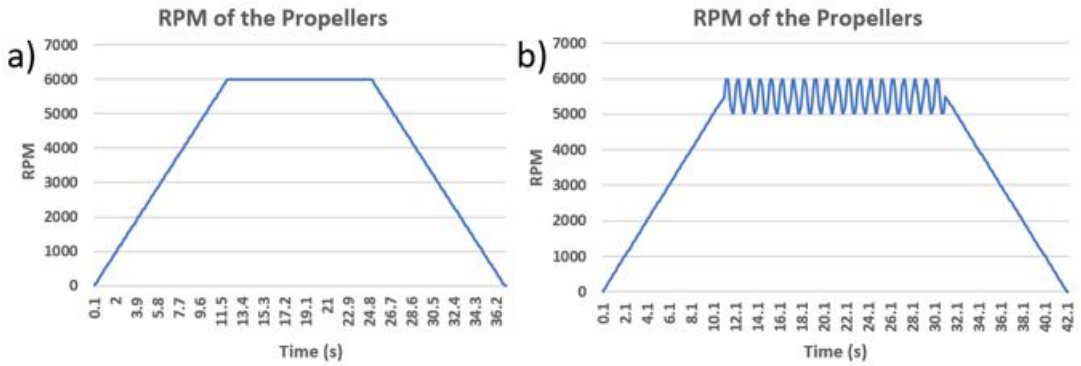

Figure 25: Example of two different scenarios a)6000 RPM constant b) sine function varies between 5000-6000 RPM with 1 hertz

For each case, at least five experiments are recorded. Totally, five hundred different droplets are observed in the present study. From these videos, the counts of droplet breakup occurrence are collected. As expected, using faster propellers creates stronger turbulence which can breakup more droplets.

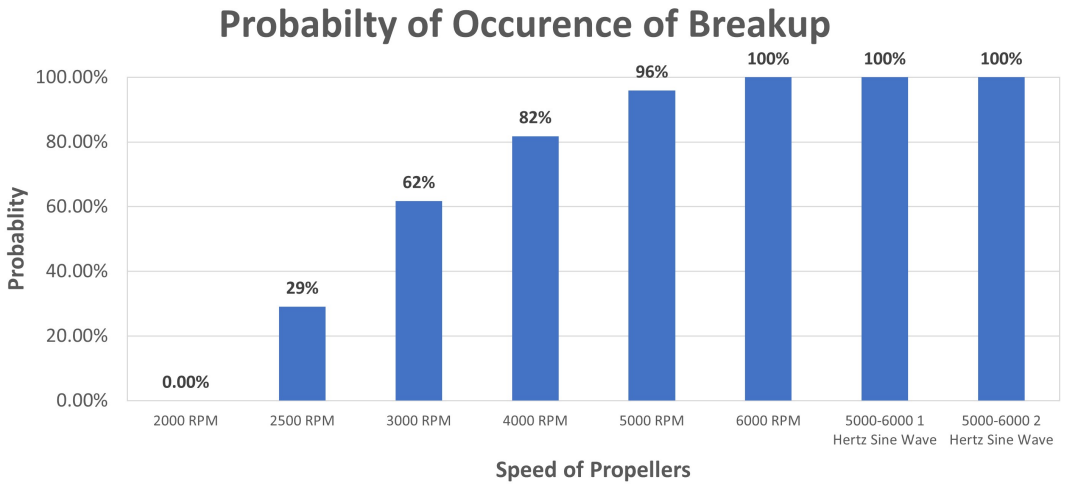

Figure 26: Probability of occurrence of droplet breakup respect to different velocity profiles

The probability data from any experiment cannot contain a confidence interval which estimates plus and minus of the variation in those trials. In order to conduct ant statistical test or procedure, the data must be a simple random sample, chosen independently and includes at least 15 success and failures [25]. For example; the probabilities of the droplet breakup events are random variables and has a mean of 'p' and include number of trials 'n'. The standard deviation of the data is as following;

$$SD = (p(1-p)/n)^{0.5} \tag{23}$$

The margin of the error can be estimated by supposing that the experimental data is normally distributed with 95% confidence as in usual scientific research [26]. By assuming that the 95% confidence level, the z-score 'z*' can be selected as 1.96 to find the standard error by multiplying it with margin of the error, known as SD.

The standard error leads to observe the maximum and minimum probability of the breakup occurrence.

$$\text{Standard error } = +/- z^{*}(\mathrm{p}(1-\mathrm{p})/n)^{0.5} \tag{24}$$

In the next table, the probability range for the droplet breakup events by adding and removing the standard error from the experimental probability.

Table 13: Detailed information about count of the produced droplet and probability of breakup occurrence

Servo Motor Scenario	Number of Produced Droplets	Number of Breakup Occurence	Probability of Break up Occurrence	Standard Error	Minimum Probability	Maximum Probability
2000 RPM	37	0	0%	0%	0%	0%
2500 RPM	55	16	29%	12%	17%	41%
3000 RPM	68	42	62%	12%	50%	73%
4000 RPM	66	54	82%	9%	73%	91%
5000 RPM	74	71	96%	4%	91%	100%
6000 RPM	77	77	100%	0%	100%	100%
5000-6000 RPM 1 Hertz	62	62	100%	0%	100%	100%
5000-6000 RPM 2 Hertz	60	60	100%	0%	100%	100%

As mentioned, whole propellers push the air flow towards the center with same velocity, but it must be ensured that the flow is non-directional. By dividing the observation area at its center, it can be observed whether the droplet breakup on the right or on the left due to manufacturing or assembling problems which effects the rotation of propellers. On the other hand, observing the height, where the droplet breakup, is a significant information to measure the turbulence around it with hot wire. Also, the data from numerical studies are taken for 3.5 cm far from the center to each direction. The information from analytical approach can be considered and applied only for this height gap. In addition, a high-speed camera (Photron Fastcam Nova S6) connected near to window of the wind tunnel. The videos are recorded with 6400 FPS. Two different light sources are placed nearby to camera and opposite of the camera due to display the lower levels begins after 22 cm. A paper sheet is used to lower the light of the opposite one.

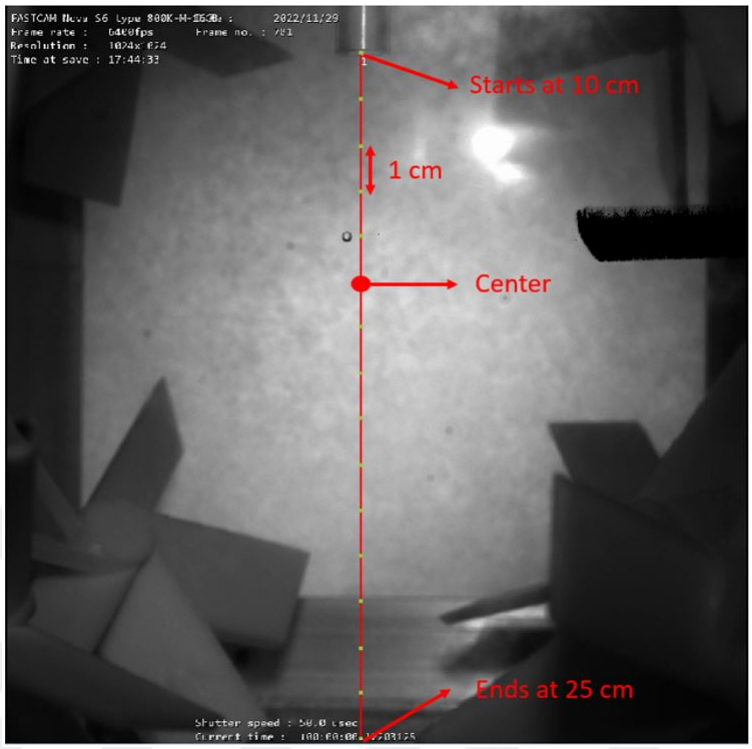

Figure 27: Frame of the collected images with height measuring line

For the present study, although the droplets are directed to right more than left, the difference is decreased as much as possible by being sure about concentric placement of moving parts.

The height placement of droplet breakup occurrence is expected at near the center of wind tunnel. However, especially for low RPM values as 2500 and 3000 RPM, there are more breakups near the edges of the test cell where the flow is stronger and directs inward as in Figure 29. In addition, diameter of the droplet is measured with respect to average of diameter lines on x and y axis by referencing the diameter of the plexiglass tube.

For the present study, the main goal is to observe non-directional or multi-directional breakup due to investigation of turbulent effect. Therefore, velocity profiles should allow the droplet breakup to be seen closer to the center. In the Figure 30, the higher lines on the left of the graph may indicate that the breakup is caused by turbulence.

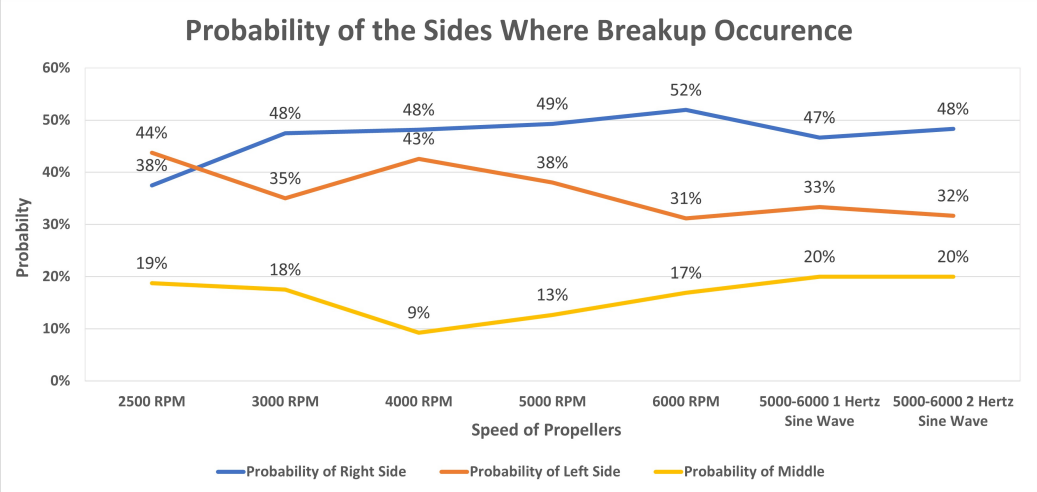

Figure 28: Probability of the sides where the breakup occurred

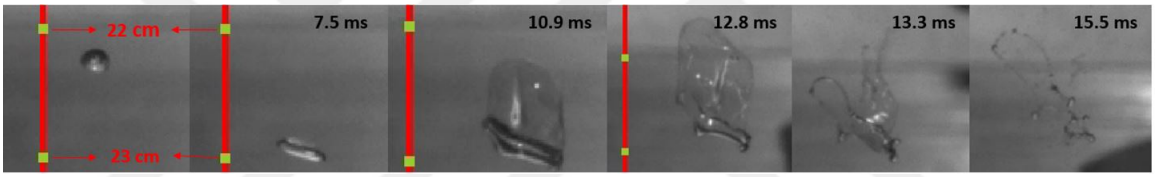

Figure 29: An example of a breakup, directed to the center (speed of the propellers: 3000 RPM, diameter of the droplet: 2.11 mm, type: bag breakup)

The probability of these lines, placed near the center, is higher for 5000-6000 RPM cases.

By using the same color code for 5000 and 6000 RPM cases, the sine-based velocity profile with 1 and 2 hertz and oscillating between these RPM values are compared in the Figure 31 to observe the most observed height range. The height of the breakup appearances becomes lower but still not much near to the center. As in the graph, the 40 percent of the breakup data can be collected between 19-22 cm. Besides that, only 12.5 percent of the breakups are happened between 14-17 cm where the center is placed on 15th cm. Therefore, the wind condition between 19-22 cm must be measured with the hot wire.

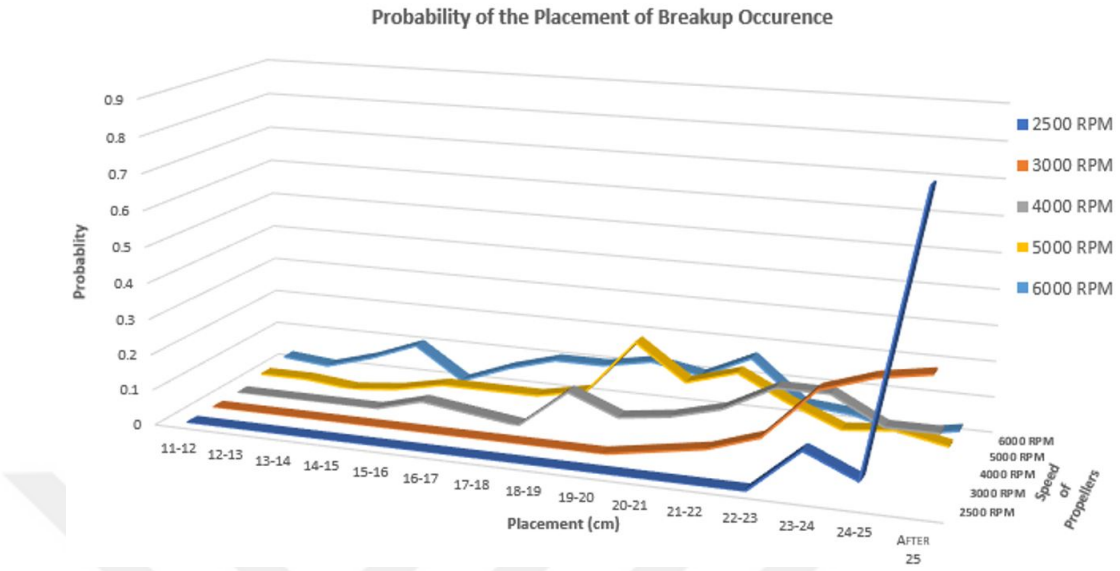

Figure 30: Probability of the height ranges where the breakup occurred in constant speed of propellers

Table 14: Detailed information about counts of the most probable breakup height and its probability for each scenario

Servo Motor Scenario	The Most Probable Breakup Height Range	Count of the Probable Breakup Height	Number of Breakup Occurrence	Probabilty of the Probable Breakup Height Range	Standart Error	Minimum Probability	Maximum Probability
2000 RPM	-	-	-	-	-	-	-
2500 RPM	After 25	13	16	81%	19%	62%	100%
3000 RPM	24-25	12	42	29%	14%	15%	42%
4000 RPM	23-24	10	54	19%	10%	8%	29%
5000 RPM	19-20	16	71	23%	10%	13%	32%
6000 RPM	21-22	13	77	17%	8%	9%	25%
5000-6000 RPM 1 Hertz	22-23	9	62	15%	9%	6%	23%
5000-6000 RPM 2 Hertz	22-23	9	60	15%	9%	6%	24%

The breakup appearances are investigated with four parts to determine the type of the breakup as vibrational, bag, multiple and unknown. The multiple refers to a breakup which is firstly appeared as vibrational and the smaller droplets from this breakup are disintegrated as bags. In addition, some of the breakup events cannot be specified due to stochastic phenomena of the wind condition and lack of knowledge about whole breakup types.

For the constant operating RPM values, the probability of bag and multiple

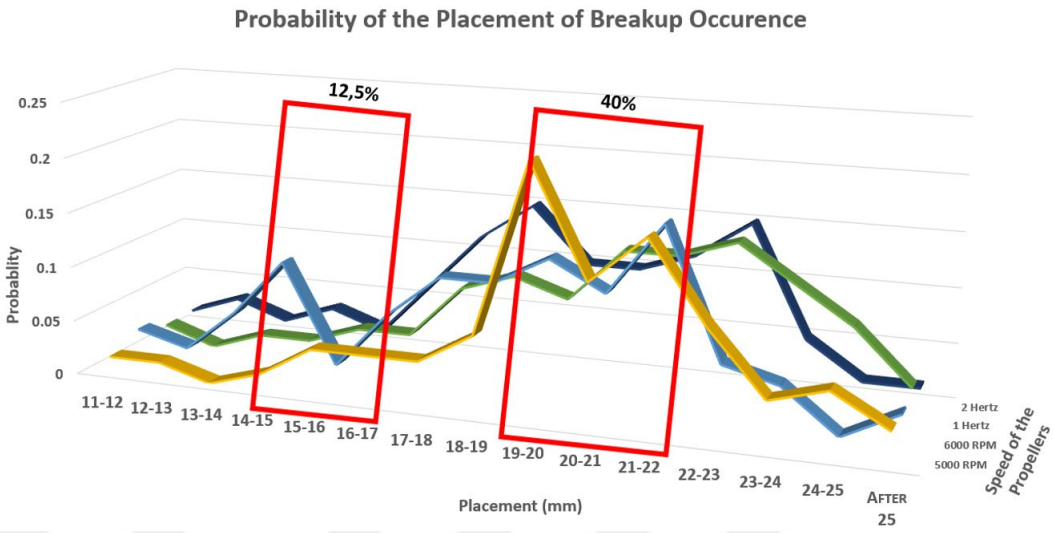

Figure 31: Probability of the height ranges where the breakup occurred in different velocity profiles

breakups increases by speeding up the propellers but the probability of the vibrational breakups decreases. This relation can be described that the higher Taylor Reynolds number leads to bag breakup rather than vibrational breakup because of the stronger momentum source. In addition to this, increasing the frequency of the sine function provides more multiple and vibrational breakups which is quite interesting. These two scenarios have the same height range for the most breakup events, however breakups before 22nd cm is more for 1 Hertz application. Therefore, the turbulent Weber Number for 1 hertz application can be less than the 2 hertz due to lower speed of the droplet which is gained due to impact time of gravity.

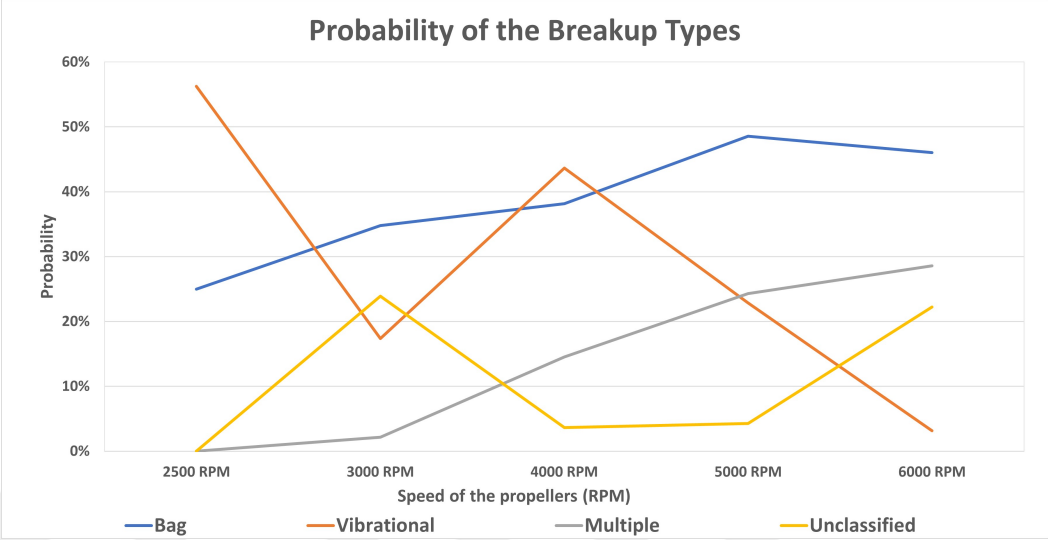

Figure 32: Probability of the breakup types in constant RPM values

Table 15: Probabilities of the droplet breakup types for each scenario

Servo Motor Scenario	Vibrational Breakup				Bag Breakup			
	Probability in Experiment	Standard Error	Minimum Probability	Maximum Probability	Probability in Experiment	Standard Error	Minimum Probability	Maximum Probability
2500 RPM	56%	13%	43%	69%	25%	11%	14%	36%
3000 RPM	17%	9%	8%	26%	35%	11%	23%	46%
4000 RPM	44%	12%	32%	56%	38%	12%	26%	50%
5000 RPM	23%	10%	13%	32%	49%	11%	37%	60%
6000 RPM	3%	4%	0%	7%	46%	11%	35%	57%
5000-6000 RPM 1 Hertz	5%	5%	0%	10%	58%	12%	46%	71%
5000-6000 RPM 2 Hertz	10%	8%	2%	18%	40%	12%	28%	52%
Servo Motor Scenario	**Multiple Breakup**				**Unclassified Breakup**			
	Probability in Experiment	Standard Error	Minimum Probability	Maximum Probability	Probability in Experiment	Standard Error	Minimum Probability	Maximum Probability
2500 RPM	0%	0%	0%	0%	56%	13%	43%	69%
3000 RPM	2%	3%	0%	6%	17%	9%	8%	26%
4000 RPM	15%	9%	6%	23%	44%	12%	32%	56%
5000 RPM	24%	10%	15%	34%	23%	10%	13%	32%
6000 RPM	29%	10%	18%	39%	3%	4%	0%	7%
5000-6000 RPM 1 Hertz	25%	11%	14%	36%	5%	5%	0%	10%
5000-6000 RPM 2 Hertz	33%	12%	21%	45%	10%	8%	2%	18%

To enhance the explanation of the breakup behavior, images from different scenarios, which is selected for ease in understanding, shared about different breakup types. In the Figure 34, a vibrational breakup can be seen by rotating itself respect to varying axis. Firstly, it starts to turn around at y-axis but the rotation axis is changing through a z-axis until it breaks up. Also, the smallest droplet at 66.25 ms goes in a different direction to others.

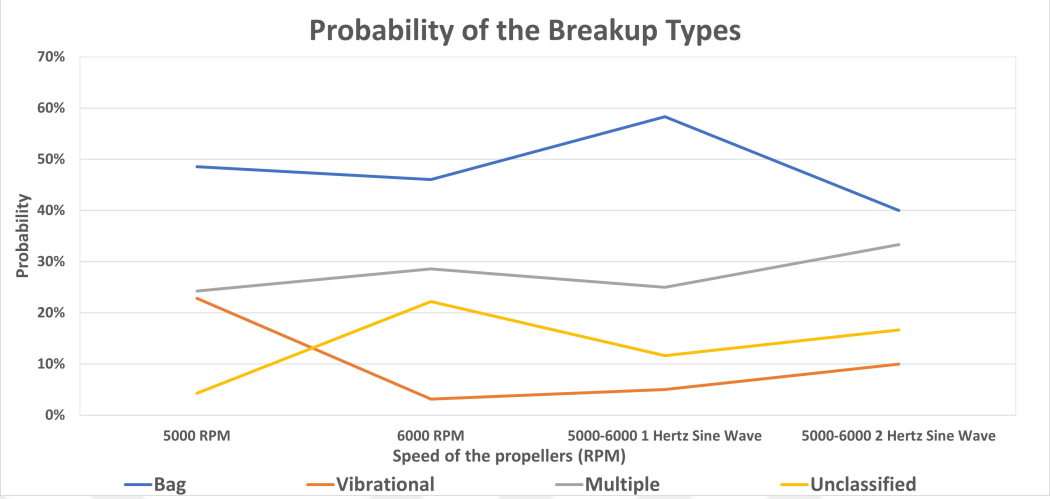

Figure 33: Probability of the breakup types in different velocity profiles

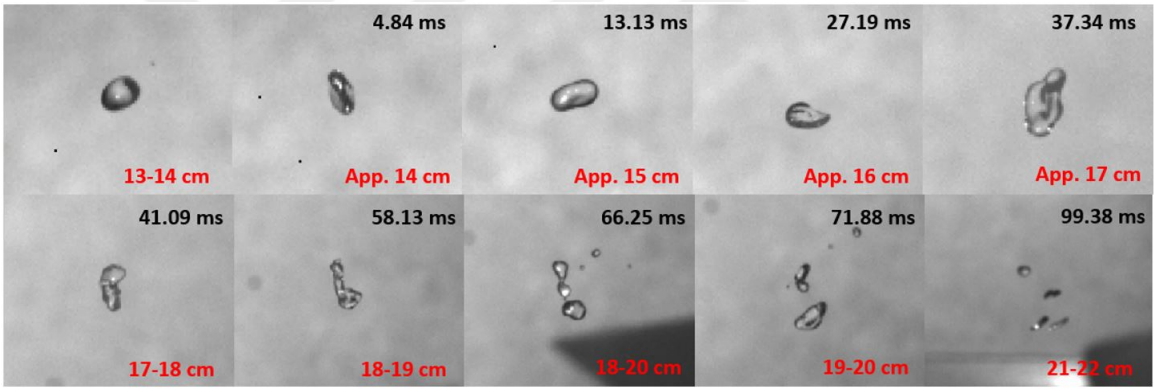

Figure 34: An example for a vibrational breakup (speed of the propellers: 5000 RPM, diameter of the droplet: 2.32 mm)

The vibrational breakup can cause a bag breakup within self, due to thinning the droplet through a fragile liquid film. In the example of Figure 35, the droplet starts the turning around itself like the previous breakup example after 14th cm but the provided force is still not enough for dividing the droplet. After starting of the vibrational breakup, the thin layer goes to right direction and two bag structures occurs in same direction. While the upper part of the droplet has a vibrational breakup behavior, the lower part starts to disintegrate within a bag structure. In addition, the smaller droplets are distributed through each direction.

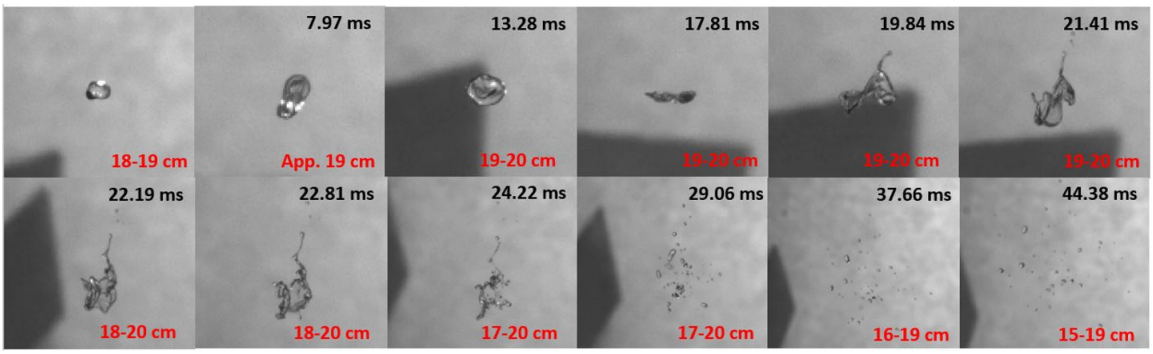

Figure 35: An example for a hybrid breakup (speed of the propellers: 6000 RPM, diameter of the droplet: 2.19 mm)

For the bag breakup structures, if the direction of breakup process changing during total disintegration, a turbulence effect can be observed due to non-directional flow. Many of bag breakups in sine function cases tend to diverse the directions with different bags or the same bag. Especially in the Figure 36, the droplet becomes a thin shape in a certain direction of +y axis but the first bag occurs in between directions of north and north-east of the frame. It can be seen that there is a direction change for this bag with breakup in +y direction before the other breakup. In addition, a small bag formed through absolutely in east direction by the change of the wind. Due to thinness of the liquid film, this bag structure cannot live much longer than others and disintegrates immediately. However, observing changes in the direction of the breakup structures leads to think that there should be a non-directional turbulence.

The multiple breakup consists of bag and vibrational breakups one after one of them occurred. In most of the experiments with the observation of multiple process, smaller droplets from vibrational breakup goes through right, left or bottom sides where the flow is stronger due to main flow which is caused by side flow of the propellers. Two flows with similar properties are collapsed and collided to each other and directed to the center of the wind tunnel. However, there a few examples of multiple breakup where the time difference between vibrational and bag breakup is little as much 2-3 ms. In the Figure 37, the droplet disintegrates at time 24 ms

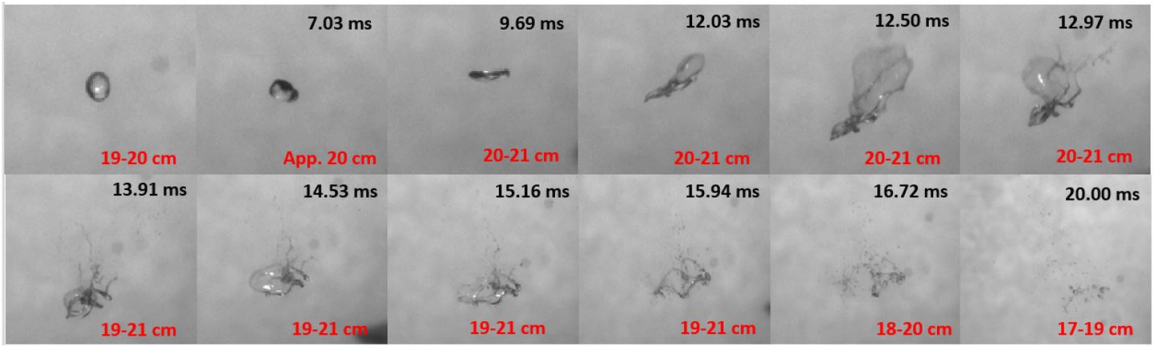

Figure 36: An example for a multi-directed bag breakup (speed of the propellers: 5000-6000 RPM sine func. 2 Hertz, diameter of the droplet: 2.03 mm)

vibrationally by rotating itself. After a short time, a strong flow conditions came from bottom side of the test cell and breakups the smaller two droplets with bag structure.

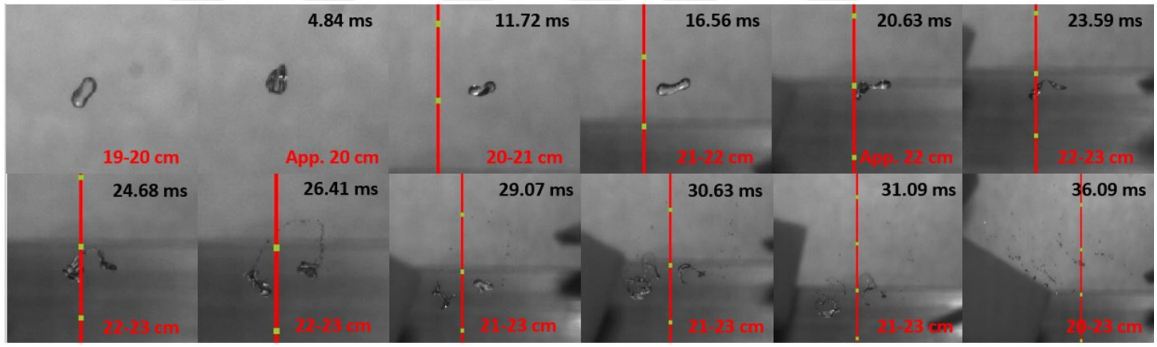

Figure 37: An example for a multiple breakup (speed of the propellers: 5000-6000 RPM sine func. 1 Hertz, diameter of the droplet: 2.00 mm)

The data of the videos and the velocity profiles from feedback system of the servo motors are recorded to combine the information between the turbulence conditions near the droplet. Since the starting of the experiments, increasing speed of the propellers rises the probability of occurrence of the droplet breakup. Besides changing the speed in short times by using sine waves display more interesting droplet behaviors. In order to investigate the relations of whole parts in the study, 6000 RPM case can be a solution by providing the most droplet breakup appearances in between 14-16

cm where the center is nearby. In addition, the numerical and analytical approaches are done according to the specified displacement.

4.2 Turbulence Measurements of the Wind Tunnel

The flow condition in the test chamber is measured with the velocity by using a hot wire system which is placed at the center. A Dantec Dynamics 54T42 hot-wire anemometer device with one 56P16 4-m cable-equipped wire probe were used. The voltage data is measured and collected with NI (782258) Multifunction DAQ. The records contain 60 sec of voltage data with 30000 samples per seconds. The voltage data were collected with 6 different records for 10 sec durations to provide a 60 sec data with 1.8 million data in it. For each 10 sec records, there are 2 sec gaps between saving the voltage data. Whole 60 sec data were collected during where the wind tunnel continued to work with the same operating conditions of fan and servo motors.

In the test section, a 12V computer fan was utilized as a flow source by changing its speed respect to the given voltage. The working voltage gap is between 3-12 V. Therefore, 10 different experiments have done by increase the voltage value with 1 V for each experiment. In addition, a measurement when the fans are stopped, is taken, and placed to zero value of the velocity. For the calibration process, the static pressure difference between the entrance and the exit of the contraction of the test section was measured. The pressure difference can be easily converted to velocity at the exit by using the Bernoulli equation and the law of conservation of mass. The collected velocity values are used as reference points according to measured voltage values from hot-wire probes. The probe was positioned in two different directions, as shown in Figure 38, to increase the capability of measuring different directions of the velocity.

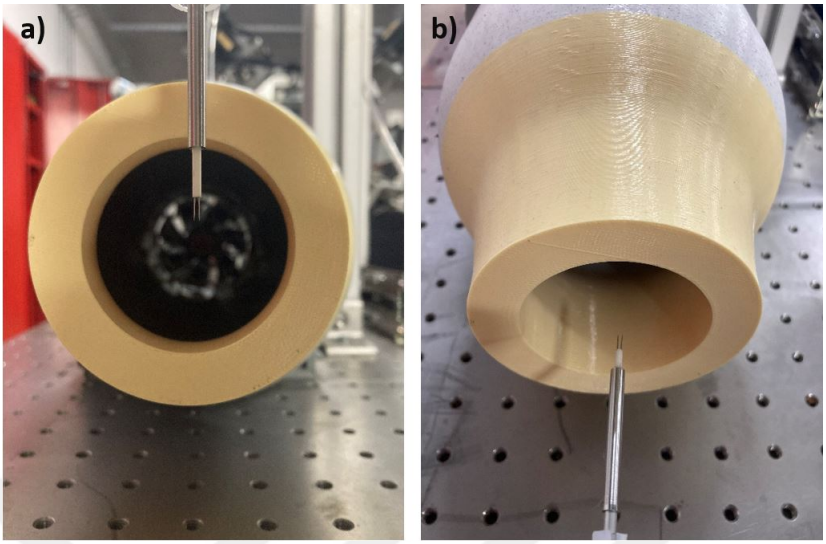

Figure 38: Placements of hot-wire probe: a) Vertical, b) Horizontal

4.2.1 Calibration of the Hot-wire Probe

The measured signal potential, $E(t)$, has a relation with the effective cooling velocity, $U(t)$, where the wind flows perpendicularly to the wire probe. By using the relation of the Bruun, the relation can be expressed as following [27]:

$$E(t)^2 = A + BU_e(t)^n \tag{25}$$

This equation represents a linear relation by finding the calibration parameters as A, B and n which are independently valid for each probe position. For the calibration of the wires, the mean value of the cooling velocity and voltage were utilized to calculate calibration parameters.

$$\bar{E}^2 = A + B\bar{U}_e^n \tag{26}$$

The velocity calibration data for two different positions were collected separately and interpolated to find a middle curve to apply for whole positions of measurements in the wind tunnel. The calibration parameters and r-square value can be seen in

the graphs. In addition, the curve is enlarged to observe higher velocities than the calibration cases.

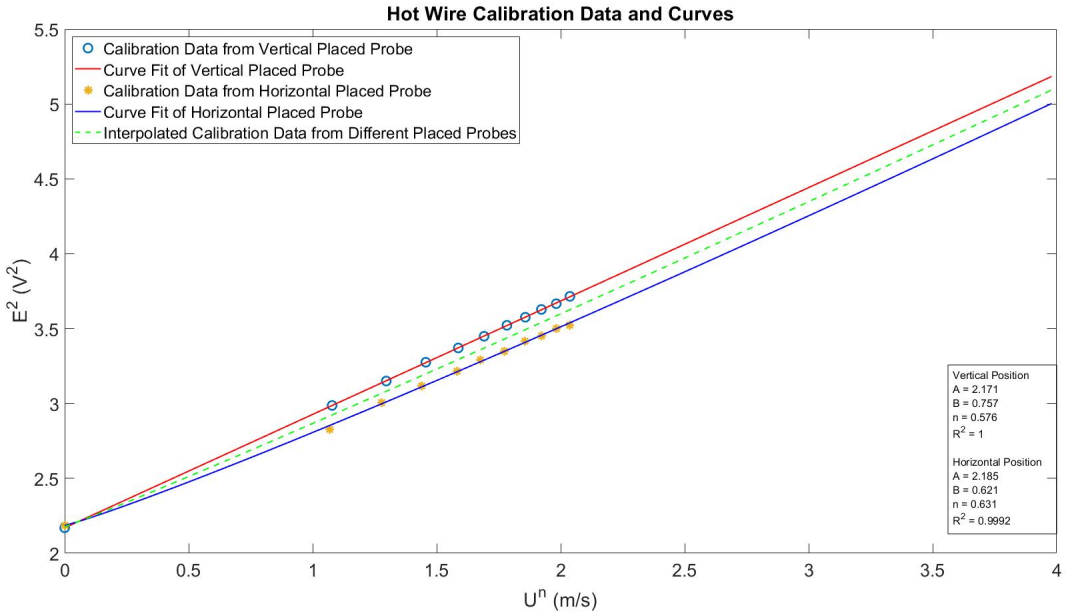

Figure 39: Hot-wire calibration curve to be used in converting the voltage to velocity magnitude

4.2.2 Hot-wire Measurements in the Wind Tunnel

The hot-wire probe places in the plexiglass tube same as the syringe needle. Also, the plexiglass tube connects to the wind tunnel and the table which holds the tunnel because of occurrence of high vibration during working process. In order to measure the flow properties at the center of the tunnel, the probe is fixed to be in 150 mm far away from the upper cover. Direction of the probes changed by 90 degrees for two different cases as named as parallel to glass (PG) and parallel to cover (PC). The positions are shown in the Figure 40.

The PG placement measures a flow with the domination of the flow from the direction of the glass opposite of the probes. Also, the same behavior occurs in the PC placement which is mostly affected by the flow from the direction of the cover due

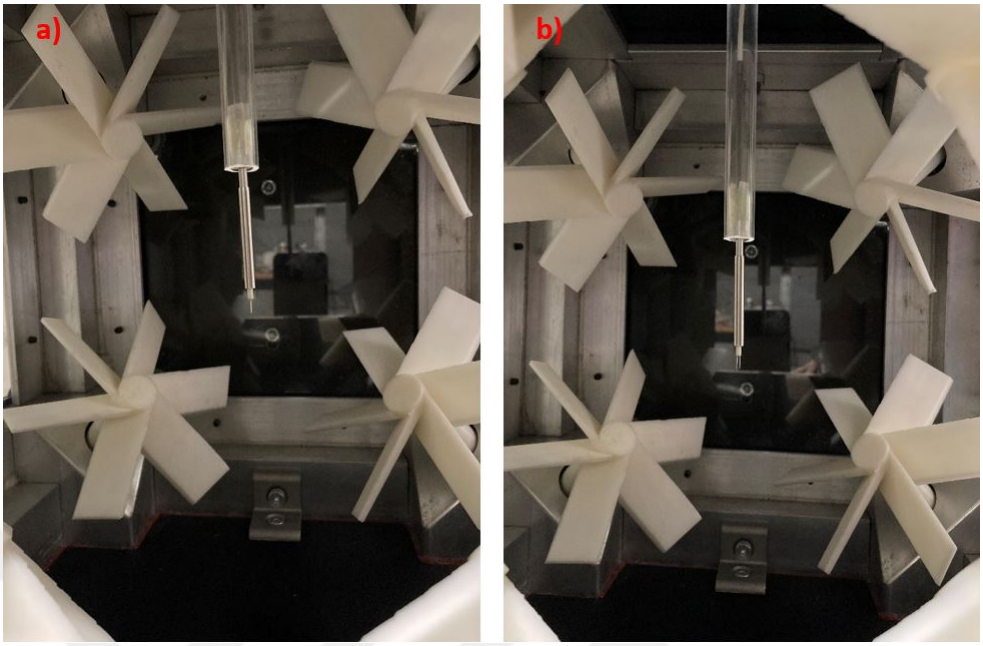

Figure 40: Position of the hot-wire probes: a) Parallel to glass (PG), b) Parallel to cover (PC)

to nature of the convective cooling phenomenon. Because the surface area changes for wind from several directions. As in the LES simulations, the air flow can hit to probe in several directions and cool the probe randomly. Comparing the difference between these two positions leads to observe the isotropy of the system as well. From the assumption of isotropic flow, the probes have not placed on lateral direction into the tunnel.

4.2.3 Results of the Hot-wire Measurements

The experiments are stored in 60 sec, as explained at the beginning of this chapter, for each servo motor scenario. To explain the processing of the data, one case is selected to investigate deeply in this report. However, the calculation process is same for other scenarios. For the case of 6000 RPM (PC), the voltage data and the velocity magnitudes derived from calibration curve function, are given in Figure 41.

The turbulent intensity is calculated for each time step and averaged respect to

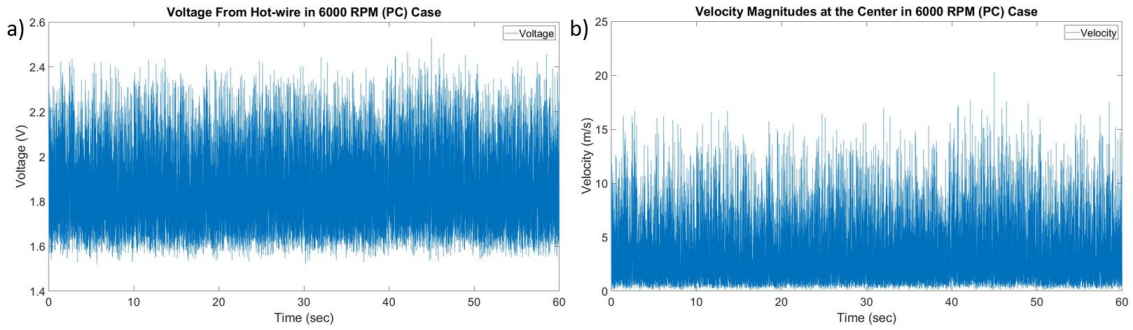

Figure 41: Voltage data and the obtained velocity magnitudes at the center of the tunnel; a) Voltage data, b) Velocity magnitudes

total time by fluctuating velocity divided by the mean velocity. The mean velocity magnitude and turbulent intensity for different servo motor scenarios leads to a difference. Higher RPM value leads to higher mean velocity rather than higher frequency application.

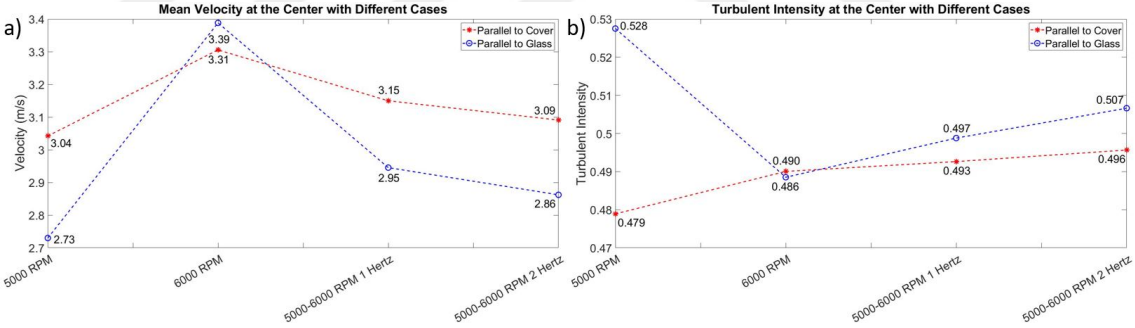

Figure 42: Mean velocity and turbulent intensity at the center of the tunnel; a) Mean velocity, b) Turbulent intensity

In order to investigate the homogeneity of the flow, similar turbulent intensities from different positioned probes leads to similar flow conditions from different directions. Finding velocity magnitudes at the center leads to find the turbulent kinetic energy and turbulent dissipation rate by using power spectrum density with the same method, as in numerical approach, given in Eq.11 and Eq.13. The Welch's power spectral density estimation with "pwelch" command in MATLAB, is used with window size of 30000 and number of overlapped samples is 10000. The PSD results

respect to frequency and wave number is shown in Figure 43.

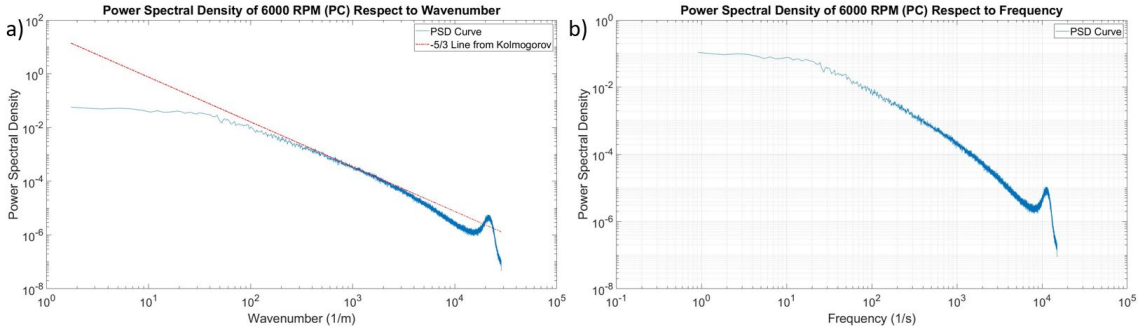

Figure 43: Power spectrum density curves of 6000 RPM (PC) case with -5/3 line a) PSD respect to wavenumber, b) PSD respect to frequency

In the PSD graphs, high frequency noise can be seen over 12000 Hz. Like any other experimental equipment, the level of this noise corresponds the high freq. noise at minimum resolution level. This noise can be neglected, since the -5/3 curve fits well and shows that energy containing large scale eddies could be resolved.

According to PSD curves above, the turbulent kinetic energy and turbulent dissipation rate for each case are calculated and compared as in following figure. In addition, comparing the TKE value with the 'uu' magnitude, calculated by using Eq.12, leads to find more reliable result from power spectrum density when the magnitudes are closer. The difference can be decreased by changing the window size and number of overlaps in the Welch's method.

The turbulent kinetic energy is increasing with the rise of RPM value. The sine wave with higher frequency provides less kinetic energy which gives a clue for having larger eddies due to high time scale of the propeller. On the other hand, the TKE and uu values are enough similar to detect the correct sizes for window and number of overlaps for power spectrum density. TKE and TDR are required to estimate the length scales and Taylor Reynolds number of the flow. By using Eq.5-6-7-8-9 with respect to the obtained TKE and TDR, the turbulent properties of the wind conditions were observed as shown in Figure 44.

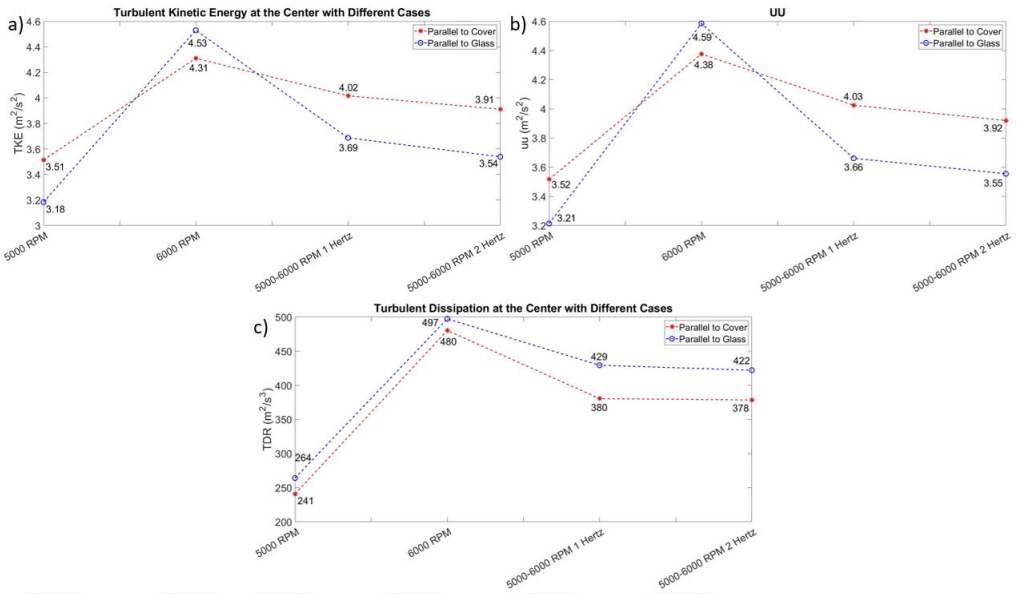

Figure 44: Turbulent kinetic energy (TKE), uu and turbulent dissipation rate (TDR) values for whole scenarios; a) TKE, b) TDR, c) uu

As expected, higher RPM values creates smaller eddies and Taylor Reynolds number follows the same pattern. However, with more time scale of the propeller in low frequency, bigger eddies are occurred. For an example, tip of the propeller blades cut the flow as a line of spaghetti and the lower frequency motion of the blades leads to longer spaghettis. Providing smaller vortices on the droplet might build more catastrophic environment to reach smaller daughter droplets. In addition, for each scenario, Taylor microscale is low enough to influence the droplet by creating a pressure difference on the liquid surface. Therefore, the breakup experiments can show the effect of forces of small vortices and the time of droplet spends in turbulence flow causes more difference of forces acting on the various point on surface and in several directions.

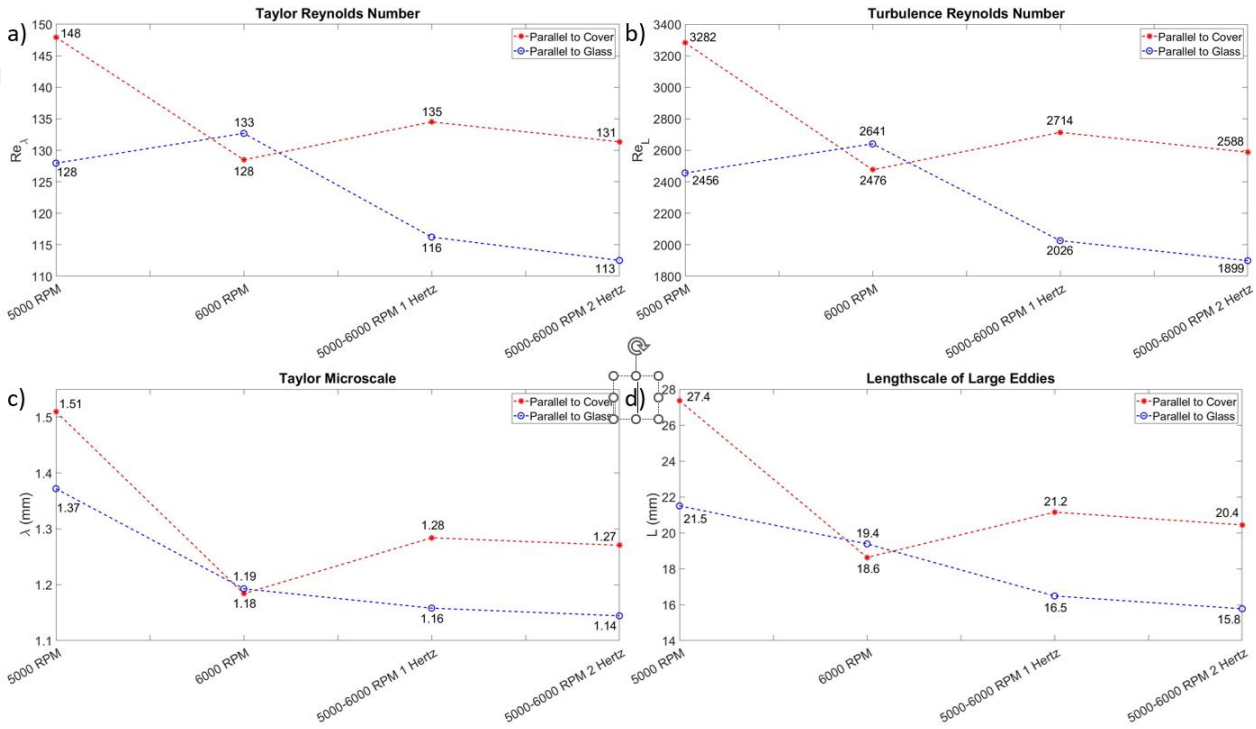

Figure 45: Calculated turbulence properties at the center of the tunnel respect to different scenarios; a) Turbulence Reynolds number, b) Taylor Reynolds number, c) Taylor microscale, d) Lengthscale of large eddies

CHAPTER V

CONCLUSION AND FUTURE RECOMMENDATIONS

5.1 General Conclusion

A new experimental system is built and interaction between turbulent flow and droplet was investigated respect to other parameters rather than only turbulent dissipation rate and surface tension. The wind tunnel can breakup ethanol droplets of 2 mm diameter.

In the present study, a cubic shaped wind tunnel is designed with CFD method and analytical perspective to define the turbulent quantities. The provided turbulent flow must be breakup a single droplet and the results from CFD and analytical studies show that the system can breakup 2 mm water and ethanol droplets. The turbulent flow is highly isotropic and homogenous respect to velocity data from 109 probes. The experimental setup is built according to results from CFD and analytical calculations. In addition, nearly 2 mm diameter droplets were produced with syringe pump. Needle of the syringe placed into plexiglass tube to be close to center of the test cell. The droplets should spend its time as much as in the center of the system where the isotropic and homogeneous turbulent flow is achieved.

The experiments includes several velocity profiles, droplet breakup type and different turbulent quantities. Increasing the speed of the propellers, increases the turbulent kinetic energy and dissipation rate which causes to observe more droplet breakup. However, higher frequency motion of the propellers provide less amount of kinetic energy and dissipation rate. The same relation works also for length scales.

The CFD method by using LES method with a set of analytical solutions creates stronger turbulence with higher turbulent kinetic energy and dissipation rate. There

are three different aspects, that can define the difference, which are CFD method, analytical approach and hot-wire. The turbulent quantities, especially for literature view and experimental results, are calculated according to Pope's book [18]. The set of equation is for a perfect isotropic and homogeneous turbulent which includes equivalences from hypothesises of Kolmogorov and Taylor. Also, the power spectrum density approach cannot contain the whole eddy structures. The turbulent kinetic energy and dissipation rate values are found quite less in the literature examples and the wind tunnel. In the case of the present wind tunnel, the calculated dissipation rate from measurements with hot wire, must be much higher to breakup 2 mm droplets of water or ethanol respect to Hinze's work [17]. The Hinze's work is not an exact solution but the difference is in order of magnitudes which should not be explained only with Hinze's D_{max} definition. As expected due to mean velocity magnitude results from CFD and hot-wire, the turbulent kinetic energy values lead to observe the less amount of dissipation rate. On the other hand, the LES method can generate larger eddies and avoid the smallest scale which increases the these two turbulent quantities at the same time. In addition, measuring the velocity with its components help to understand the difference clearly rather than velocity magnitudes. To sum up, the CFD method can generate higher turbulent kinetic energy and dissipation rate which are measured and calculated with several methods rather than measuring and investigating with course analytical equations only with velocity magnitude.

For the breakup process, especially the first breakup example in Figure.34, the droplets are continuously forced by the turbulent flow as observed in the experiments by losing their circular shape. Mostly, the droplets starts to rotate and after breakup in any type. The duration before breakup occurrence has a significant effect on breakup by forcing the droplet surface. Therefore, the syringe pump was used at near to the center. Because, fast droplets can not breakup in the system. The reason lays behind the time scale and vortices which acts on the droplet with its journey in the

flow. The continous deformation process helps in break up process by changing the direction of the forces which shakes and streches the droplet.

The breakup types are separated and classified in, as in the Table.1, work of [1]. However, different breakup types were observed in the wind tunnel. In the Figure 35, top part of the droplet disintegrates in vibrational type but there are two bag structures were occurred at the bottom part and breakup at the same time. It claims that there should be hybrid regimes for classifying and modelling the droplet breakup. Also, there is a sudden change in different breakup types as in Figure.37. According to described breakup models in the introduction, droplet divides into two smaller droplets and the models might be stop working for breakup in such examples. Therefore, investigating and combining the knowledge in the relation of breakup types is a necessary work to understand the secondary atomization in a better way.

5.2 Recommendations for Future Work

The wind tunnel has the capability of applying several velocity profiles with propellers. Starting with constant RPM values are enough for primary works but the sine waves or any other wave function can create different turbulence environments. Sudden changes in propeller speed might cause smaller vortices to provide more pressure difference on the droplet surface. Also, the propellers can turn reversely which leads to intake the flow in desired direction. By using same directions for opposite placed fans, the flow might be isotropic at the same time. By doing that, the droplet can be forced with more stretched vortices due to different directed velocity field. Investigating such interesting turbulent environment can lead to create more reliable models and find a better way to atomize the droplets.

The produced and disintegrated droplets were investigated without measuring the daughter droplet size and its distribution. The interaction between the turbulence and the droplet size distribution has a key role for modelling the breakup phenomenon.

Therefore, from the on-going experiments, a image process algorithm should be built to measure and investigate this interaction.

Single droplet experiments avoids the effect of any other droplet in near surroundings even the real life applications usually includes much more of them. A droplet effect the other in the turbulent flow but there are a few studies focuses on this interaction. A drop-on-demand (DOD) device, which can produce 2 mm droplets with high repeatability and frequency, is built to create highly similar droplets for investigating the effects between them. On the other hand, using more DOD devices, droplets can be produced laterally and horizontally at the same time which displays the effects at least in 2 different directions.

Different measuring techniques can be applicable for the wind tunnel. Especially using a PIV system can provide the vector map of the flow for each time step. With this information, isotropy and homogeneity can be mapped and flow regions will be determined. The flow around the droplet can be specified and investigated carefully to understand the effects on the droplet surface. In addition, effects of the velocity profiles can be observed better with the PIV technique.

By combining the whole information from trials of several velocity profiles, multiple droplets and measurement techniques leads to a huge amount of knowledge about the interaction between the turbulent flow and atomization of a droplet. Creating specified turbulent flow environments and observing the flow field properties are a great chance to offer new effects and precise models. Even with the limited information from the current experiments will be published as a journal article.

Bibliography

[1] D. R. Guildenbecher, C. López-Rivera, and P. E. Sojka, "Secondary atomization," *Experiments in Fluids*, vol. 46, no. 3, pp. 371–402, 2009.

[2] S. Xu, S. Huang, R. Huang, W. Wei, X. Cheng, Y. Ma, and Y. Zhang, "Estimation of turbulence characteristics from PIV in a high-pressure fan-stirred constant volume combustion chamber," *Applied Thermal Engineering*, vol. 110, pp. 346–355, 2017.

[3] M. Birouk and I. Gökalp, "A new correlation for turbulent mass transfer from liquid droplets kalp," *International Journal of Heat and Mass Transfer*, vol. 45, pp. 37–45, 2002.

[4] D. Bradley, M. Lawes, and M. E. Morsy, "Measurement of turbulence characteristics in a large scale fan-stirred spherical vessel," *Journal of Turbulence*, vol. 20, no. 3, pp. 195–213, 2019.

[5] S. Ravi, S. J. Peltier, and E. L. Petersen, "Analysis of the impact of impeller geometry on the turbulent statistics inside a fan-stirred, cylindrical flame speed vessel using PIV," *Experiments in Fluids*, vol. 54, no. 1, 2013.

[6] K. S. Choi and J. L. Lumley, "The return to isotropy of homogeneous turbulence," *Journal of Fluid Mechanics*, vol. 436, pp. 59–84, 2001.

[7] S. Douady, Y. Couder, and M. E. Brachet, "Direct Observation of the Intermittency of Intense Vorticity Filaments in Turbulence," *Physical Review Letters*, vol. 67, no. 8, pp. 983–988, 1991.

[8] G. A. Voth, A. La Porta, A. M. Crawford, J. Alexander, and E. Bodenschatz, "Measurement of particle accelerations in fully developed turbulence," *Journal of Fluid Mechanics*, vol. 469, pp. 121–160, 2002.

[9] A. Lefebvre and V. McDonell, *Atomization and Sprays*. Boca Raton: CRC Press, 2 ed., 2017.

[10] N. Asghriz, *Handbook of Atomization and Spray: Theory and Applications*. Springer, 2011.

[11] G. G. Nasr, A. J. Yule, and L. Bendig, *Industrial Sprays and Atomization*. Springer, 2002.

[12] A. Frohn and N. Roth, *Dynamics of Droplets*. Springer, 1 ed., 2011.

[13] D. D. Joseph, J. Belanger, and G. S. Beavers, "Breakup of a liquid drop suddenly exposed to a high-speed airstream," *International Journal of Multiphase Flow*, vol. 25, no. 2, pp. 1263–1303, 1999.

[14] L. P. Hsiang and G. M. Faeth, "Drop Deformation and Breakup due to Shock Wave and Steady Disturbances," *J. Multiphase Flow*, vol. 21, no. 4, pp. 545–560, 1995.

[15] P. H. Clay, "The Mechanism of Emulsion Formation in Turbulent Flow," *Proc. Roy. Acad. Sci.*, vol. 43, pp. 852–865, 1940.

[16] A. N. Kolmogorov, "On the breakage of drops in a turbulent flow," *In Doklady Akademii Nauk*, pp. 825–828, 1949.

[17] J. O. Hinze, "Fundamentals of the hydrodynamic mechanism of splitting in dispersion processes," *AIChE Journal*, vol. 1, no. 3, pp. 289–295, 1955.

[18] S. B. Pope, *Turbulent Flows*. Cambridge: Cambridge University Press, 10 ed., 2013.

[19] M. S. Dodd and A. Ferrante, "On the interaction of Taylor length scale size droplets and isotropic turbulence," *Journal of Fluid Mechanics*, vol. 806, pp. 356–412, 2016.

[20] C. Shao, K. Luo, Y. Yang, and J. Fan, "Direct numerical simulation of droplet breakup in homogeneous isotropic turbulence: The effect of the Weber number," *International Journal of Multiphase Flow*, vol. 107, pp. 263–274, 2018.

[21] S. K. Soni, P. K. Kirar, P. Kolhe, and K. C. Sahu, "Deformation and breakup of droplets in an oblique continuous air stream," *International Journal of Multiphase Flow*, vol. 122, 2020.

[22] H. Zhao, D. Nguyen, D. J. Duke, D. Edgington-Mitchell, J. Soria, H. F. Liu, and D. Honnery, "Effect of turbulence on drop breakup in counter air flow," *International Journal of Multiphase Flow*, vol. 120, 2019.

[23] Ö. Ertunç, *Experimental and Numerical Investigations of Axisymmetric Turbulence*. PhD thesis, Der Technischen Fakultat der Universitat Erlangen-Nürnberg, 2007.

[24] T. de Karman and L. Howard, "On the Statistical Theory of Isotropic Turbulence," *Proc. R. Soc. Lond.*, vol. 164, pp. 192–215, 1938.

[25] R. L. Scheaffer, M. S. Mulekar, and J. T. McClave, *Probability and Statictics for Engineers*. Boston: Richard Stratton, 5 ed., 2011.

[26] National Academies of Sciences, Engineering and Medicine., *Reproducibility and Replicability in Science*. Washington DC: The National Academies Press, 2019.

[27] H. H. Bruun, *Hot-Wire Anemometry: Principles and Signal Analysis*. Oxford: Oxford Science Publications, 1 ed., 1995.

VITA

Veli Can Coşar received the B.Sc. degree in Mechanical Engineering from Ozyegin Univesity, Istanbul, Turkey in 2019 and he is currently pursuing the M.Sc. degree in Mechanical Engineering Departmen at Ozyegin Universty under the supervision of Dr-Ing. Özgür Ertunç. His research interests involve turbulent and multiphase flows.